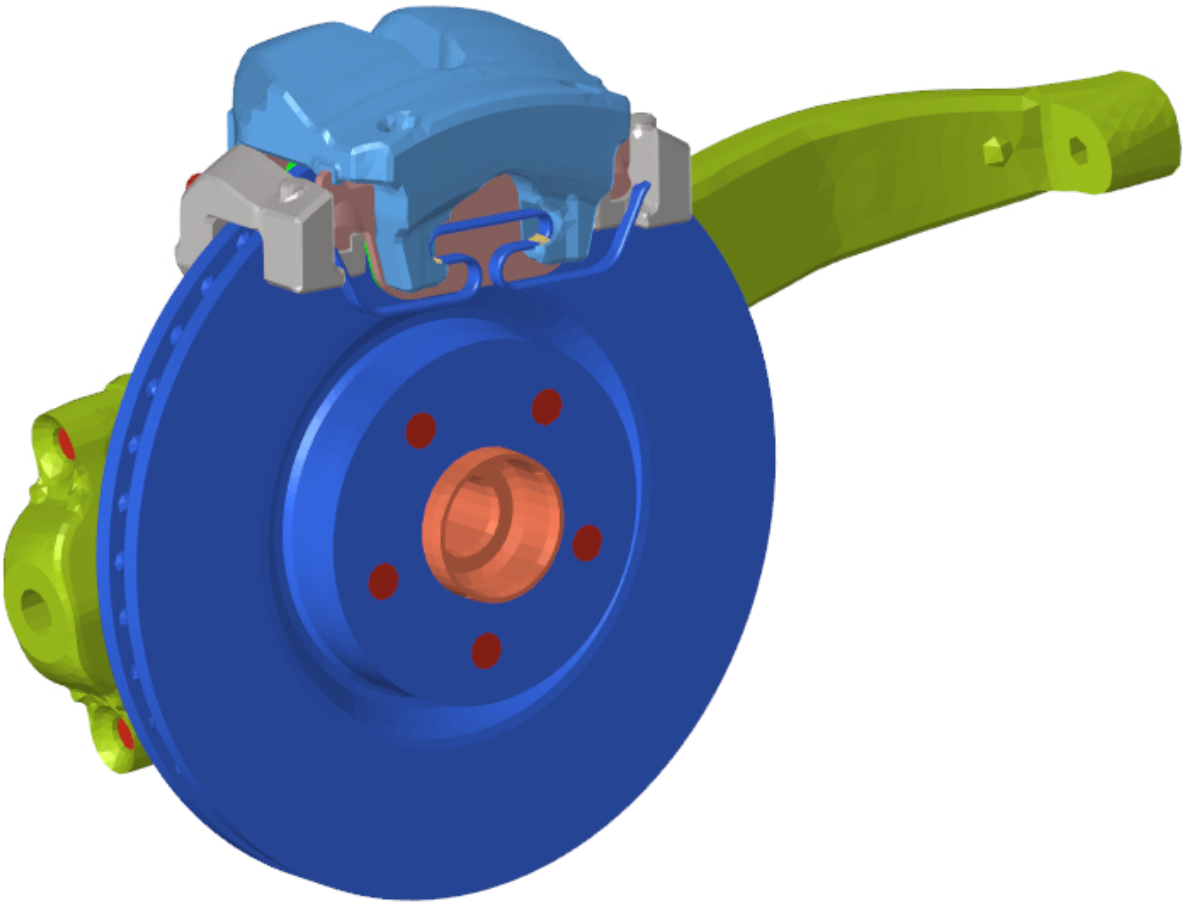

Finite Element Simulation of Energy Loss in Friction Brakes

NITESH ANIL KUMAR NIKKAM

DEPARTMENT OF MECHANICS AND MARITIME SCIENCES
CHALMERS UNIVERSITY OF TECHNOLOGY
Gothenburg, Sweden 2023
www.chalmers.se

Master's thesis 2023

Finite Element Simulation of Energy Loss in Friction Brakes

Nitesh Anil Kumar Nikkam

CHALMERS
UNIVERSITY OF TECHNOLOGY

Department of Mechanics and Maritime Sciences
Division of Vehicle Engineering and Autonomous Systems
Chalmers University of Technology
Gothenburg, Sweden 2023

Finite Element Simulation of Energy Loss in Friction Brakes
Nitesh Anil Kumar Nikkam

Supervisor: Patrick Sabiniarz, Braking, Performance and Drivability, Volvo Cars Corporation
Examiner: Roger Lundén, Professor at Chalmers Mechanics and Maritime Sciences/Dynamics

Master's Thesis 2023
Department of Mechanics and Maritime Sciences
Division of Vehicle Engineering and Autonomous Systems
Chalmers University of Technology
SE-412 96 Gothenburg
Telephone +46 31 772 1000

Cover: Finite element model of friction brake assembly established at ANSA simulation platform.

Typeset in LaTeX
Printed by Chalmers Reproservice
Gothenburg, Sweden 2023

Finite Element Simulation of Energy Loss in Friction Brakes
Master's thesis in Automotive Engineering
NITESH ANIL KUMAR NIKKAM
Department of Mechanics and Maritime Sciences
Division of Vehicle Engineering and Autonomous Systems
Chalmers University of Technology

Abstract

The focus of the automotive industry is shifting towards the development of electric vehicles due to the advances in battery technology and increasing environmental concerns. One of the main challenges with electric vehicles is "range anxiety" or the worry over the distance a vehicle can travel before needing to be recharged. Energy efficiency is therefore an important factor in improving the range of electric vehicles, and understanding the mechanisms that contribute to energy loss in a vehicle is crucial. Brake drag is one such mechanism, and it is estimated to account for around 3% of energy loss in a vehicle. Improving the energy efficiency of friction brakes can help address range anxiety and improve the overall performance of electric vehicles.

Virtual validation of brake drag torque was carried out using the finite element tool Abaqus to validate the brake drag mechanism of a friction brake assembly on both a qualitative and quantitative level. The approach involved creating an augmented model of the friction brake assembly and defining boundary conditions and contacts to simulate the behavior of the system under static conditions. A parametric study was conducted to investigate the influence of the longitudinal stiffness of the caliper housing and friction pad lining on brake drag torque. The study also included an investigation of the impact of modifying the stiffness of the omega spring. The results of the simulations were used to mimic the relationship between brake pressure and brake drag (including the "drag knee-point") and to validate the model.

The virtual environment model developed in this work can be used to quickly and accurately model and simulate different design prototypes, leading to reduced development time and optimized brake performance. The caliper housing stiffness and friction pad stiffness were found to be major factors that influence the brake drag, and the deflection behavior of the omega spring was also an important factor. It was observed that the virtual environment model can help achieve drag torque reduction with optimal brake performance. The results of the simulations were compared with existing research data and were found to be accurate. Overall, this work demonstrates the usefulness of virtual modeling and simulation in the design and optimization of friction brake assemblies.

Keywords: FEM, friction brake assembly, contact analysis, Abaqus, battery, energy loss, brake drag, range anxiety, drag knee-point, electric vehicles.

Acknowledgements

The research for the present thesis was done at the Department of Mechanics and Maritime Sciences, at Chalmers University of Technology, Gothenburg, Sweden and Volvo Cars Corporation, Gothenburg, Sweden.

First of all, I would like to sincerely thank Dr. Patrick Sabiniarz, my industrial supervisor at Volvo Cars, for the unwavering encouragement, inspiration, and direction over the course of this project. His deep expertise and suggestions for the project's next steps to be taken have proven to be of great benefit to me. Additionally, I want to thank him for fostering a friendly environment that allowed me to fit in with the staff at Volvo Cars.

I also would like to thank my examiner, Professor Roger Lundén, for his deep insights and for always being there to provide a hand. His extremely thoughtful act, his prompt email responses, and his insightful criticism motivated me to overcome the difficulties.

I am grateful to my friends for their assistance with this thesis: Varun Ramakrishnan bhardwaj, Navaneet Subbaram, Yogesh kumar and Raju Hurakadalli. Finally, I would want to express my gratitude to my parents for their support and affection throughout the years, making me able to complete my Master's program and overcome difficulties.

Nitesh Anil Kumar Nikkam, Gothenburg, March, 2023

List of Acronyms

Below is the list of acronyms that have been used throughout this thesis listed in alphabetical order:

CAE	Computer Aided Engineering
EV	Electric Vehicle
FE	Finite Element
FEM	Finite Element Modelling
ICE	Internal Combustion Engines
NVH	Noise, Vibration and Harshness

Contents

List of Figures

List of Tables

1
Introduction

1.1 Background

Strong development in battery technology along with increasing sense of environmental responsibility driven by government policies is currently shifting the focus of the automotive industry towards development of battery powered electric vehicles. Although, as compared to traditional ICE cars, an electric vehicle has multiple advantages to the consumer, the biggest concern is the "range anxiety" one faces with any electric car on the market today. Range anxiety is the "worry" over the distance the vehicle can travel before the battery needs to be recharged. Energy efficiency, a factor that influences the range of a vehicle is one of the most important factors, requiring both a holistic and detailed technical understanding of all energy dissipating mechanisms within the vehicle. One such mechanism is the drag experienced for friction brakes. This accounts to approximately 3% of the energy loss and is one of the primary contributors to energy losses experienced in a vehicle.

1.2 Problem statement

In this era of electrification of vehicles, range is the most important feature that will pull customers to a particular car model in a competitive market. To solve this "range anxiety", energy loss needs to be decreased. Since nearly 3% of this energy loss can be removed by reducing the drag on friction brakes, it is important to model and validate this phenomenon.
Hence, the goal is to calculate contribution to the energy efficiency in electric passenger vehicles through virtual validation of brake drag torque experienced for friction brakes. This brake drag torque is caused by the non-vanishing pad/disc pressure experienced after brake pressure has been released by the driver.

1.3 Objectives

1. To gain an increased understanding of brake drag on a qualitative and quantitative level in a virtual environment by building an FE model and use it for simulation.
2. Replicate and explain the generic brake-pressure to drag curve using FEM.

1.4 Deliverables

1. Finite element model to mimic generic behaviour of drag as function of brake pressure.
2. Quantify brake drag in the virtual environment.
3. To carry out a parametric study to understand the influence of various components contributing brake drag.

1.5 Limitations

- Drag is studied for a disc without rotation, i.e., static condition

  Drag is caused by non-conservative forces in the system and in this thesis these forces are assumed to arise entirely due to friction at contact interfaces. This means that, e.g., viscous material effects, that also may contribute to drag, are not considered. Influence of temperature is disregarded.

- Limitations in scope

  This is a proof-of-concept study, which means that we are only aiming at reproducing generic results in this thesis. This is the general relationship between brake pressure and drag in which a "flat section" is first encountered, followed by a steep increase when the drag knee-point is reached.

  Detailed comparison of CAE results towards measurements on the specific brake caliper will not be made.

  Correlation of data between the physical testing and the virtual environment is precluded due to unavailability of detailed test data for the specific brake caliper setup under study.

2
Theory

Drag torque is caused by the non-vanishing contact pressure between disc and pad that is encountered after the brake line pressure has been released by the driver. It arises as a consequence of non-conservative forces in the brake caliper assembly due to which the caliper does not return to its original equilibrium position after the brake pressure has been released. These non-conservative forces include primarily friction between the different components (pads, carrier, etc) of the caliper, but also material properties such as a viscous components of the stress-strain relationship. On looking closely into the mechanism of the friction brake, if the caliper deflection is greater than the maximum piston retraction (due to slip in piston and seal surface) then the running clearance is reduced to a complete zero. On the other hand, if the same parameters, i.e., the relation between caliper deflection and piston retraction are reversed, then drag is reduced to a minimum. Hence, understanding and quantifying the mechanisms by use of the FE model is very important. Quasi-static analysis is carried out with static loads applied on the system.

The relation between drag torque experienced by the disc and the brake pressure is represented on a graph where the drag torque (Nm) is measured for the brake pressure applied on the caliper. This indicates how the brake drag varies with the brake pressure at the caliper and signifies a point where there is no running clearance between pad and rotor. This is called the drag knee-point. The region beyond this point shows a drastic change in brake drag with increasing brake pressure. This generic brake-pressure to drag curve is explained in Section 2.3.

2.1 Literature study

A literature review was carried out to critically assess key friction brake components that contribute to residual brake pressure and hence drag torque. It was found that there are no adequate research or publications on FE analysis of brake drag torque. In this section, research papers of different categories found are discussed here:

- One category focuses on FE simulation of the retraction capability of rubber seal.
- Another category is concerned with modelling the actual drag in a complete caliper system using rigid body dynamics.
- A third category is concerned with test results and the influence on drag of various components, such as carrier, pad, etc.

An interesting publication by Alan Backstrom and Romteck [1] discusses design parameters influencing drag, piston retraction measurement, varying seal groove designs and the seal material properties. The interpretation of drag behaviour in relation to drag knee-point chart, in their paper, helped depicting a similar generic behavioral chart in the present project. The publication also shed light on drag measurement systems with conclusion on repeatability of the tests while correlating with the drag knee-point chart.

Parameters affecting the brake performance and overview of factors influencing drag torque are comprehensively assessed through measurement based studies explained by Achim Reich, Angelo Sarda, and Martin Semsch [2].

The work by Okon D. Anwana, Hao Cai and H. T. Chang's [3] is relevant as the FE simulation is focused on seal and caliper groove analysis. This paper emphasises on the design variations in seal and groove and their impact on piston retraction. The paper also covers the mechanism of rubber deformation within the seal groove by modelling the seal material using a hyperelastic model.

A paper on brake performance by Andrew J. Day, Hon Ping Ho and Khalid Hussain [4] explains the relation between brake pedal feel and the three potential components of the brake system, i.e, master cylinder, booster and caliper seal. The efficiency of the piston seal plays a significant role to obtain high fluid pressure and this is explained by FEM and a hydraulic system representation in the AMESim model.

The analytical study of static and dynamic FE validation and test data of the rubber seal is discussed in [5] to emphasise the effects of seal groove, caliper housing and friction lining on caliper performance. The dynamic model emphasised on all factors like the stiffness of the caliper housing, lining stiffness, groove geometry, seal material properties and dimensions affecting drag. The work by David B. Antanaitison [6] gives insights about frictional brakes operating at close proximity of brake disc rotor and frictions lining affected by brake cornering loads (i.e, in a curve). The caliper drag while cornering and braking is increased due to the loads which changes the position of the brake rotor relative to the caliper. Rotor movement is influenced by wheel bearing stiffness, wheel radius, vehicle mass, mass distribution and brake geometry at cornering. These parameters helped define a good FE model for the present project.

2.2 Friction brake

A typical friction brake system is a device that restrains motion of the vehicle by absorbing energy through means of friction. A physical model of a friction brake assembly and its components are depicted in Figure 2.1. The brakes are actuated by the brake pedal which, via a servo system, applies hydraulic pressure through a brake fluid that activates the piston which, in turn, displaces the inboard friction pad. The outward friction pads are displaced by the caliper. Hence this leads to compression of the rotor disc by the friction pads. Friction brakes operate at a very close proximity (clearance) between the rotor disc and the friction pads. Figure 2.2 defines the functionality of the components in a friction brake assembly.

The underlying physics of disc brakes lies in the application of the pressure on the friction pads through the brake pedal. This pressure is increased due to Pascal's principle and, by use of a servo system, makes it possible to transform the vehicles kinetic energy into heat energy.

A floating brake caliper contains a single piston on one side and, a pad on each side of the rotor disc. The floating caliper slides back and forth on guiding pins. On a component level, the braking can be explained by that the piston pushes the inboard disc and the caliper slides. This squeezes the outboard friction pad that brushes against the rotor causing friction braking. While the brake pressure is released there is a roll back mechanism initiated by the deformed rubber seal mounted on the caliper in contact with the piston. The rubber seal and the retraction spring systems mounted on the caliper along with the loss in brake fluid pressure retracts the pads in contact with the rotor. Figure 2.1 gives an overview of the friction brake assembly with its components used in the project.

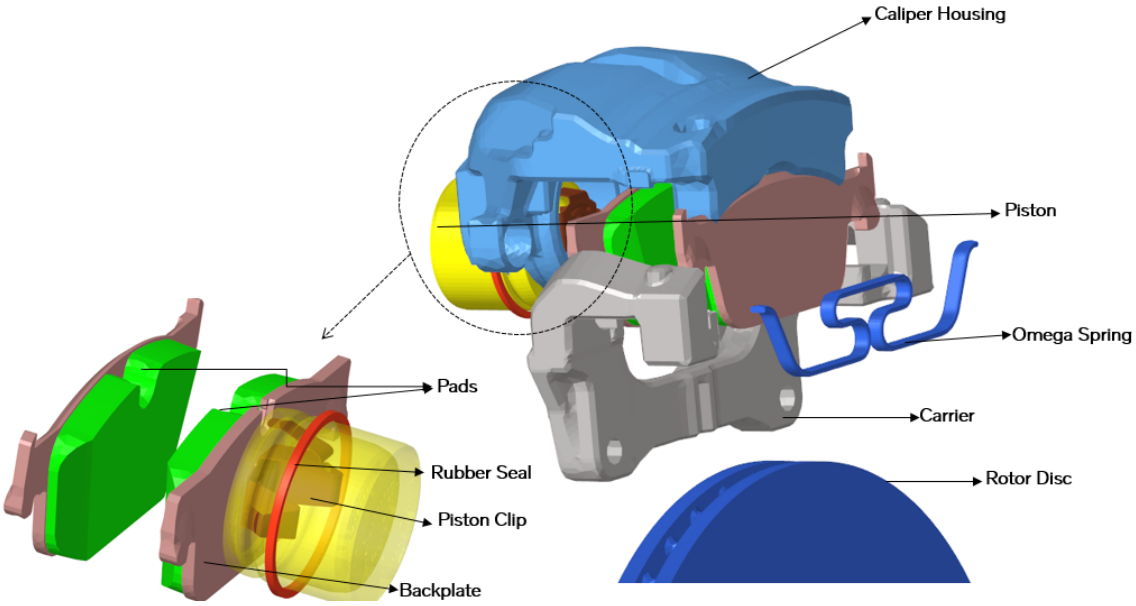

Figure 2.1: FE model of floating caliper disc brake

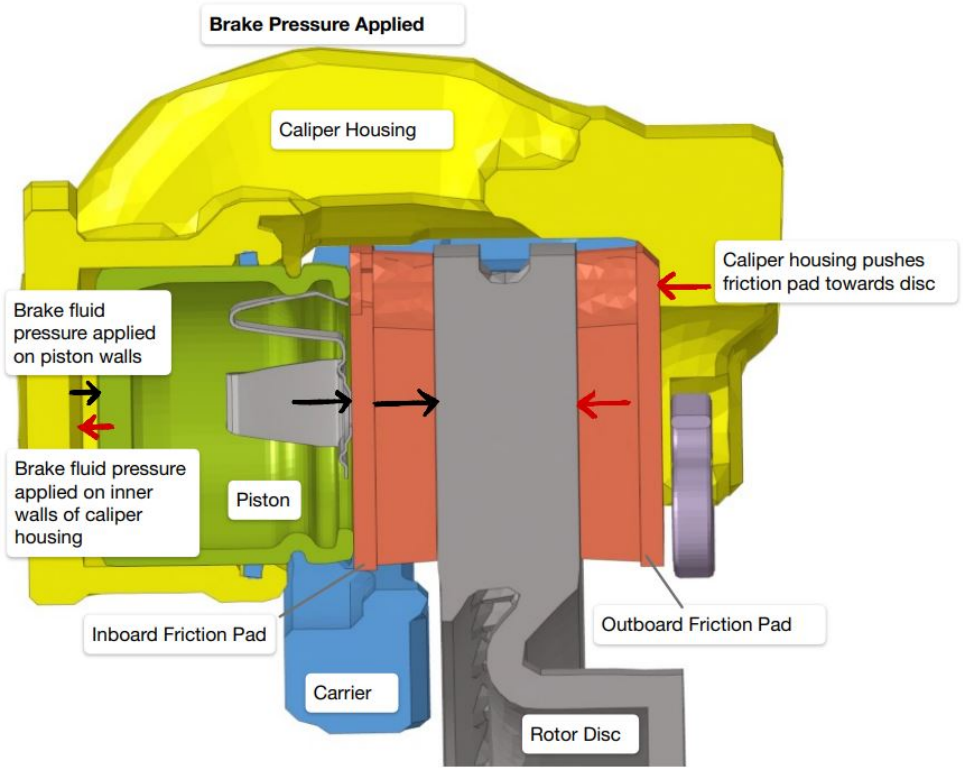

Figure 2.2: Schematic diagram of friction brake function

2.2.1 Construction

1. **Floating caliper housing**
   The caliper is a hydraulic actuator that causes movement based on the brake fluid pressure. It plays a vital role in squeezing the brake pads against the rotor. The design of a caliper is made such that it accommodates the piston. The brake caliper is clamped over the rotor as shown in figure with mountings attached to the guide pins (not seen in figure) on one side (i.e., towards the wheel unit) and the carrier on the other side. The outboard brake pad is held by a pre-tension omega spring restricting the vertical motion of the caliper as illustrated in Figure 2.3.

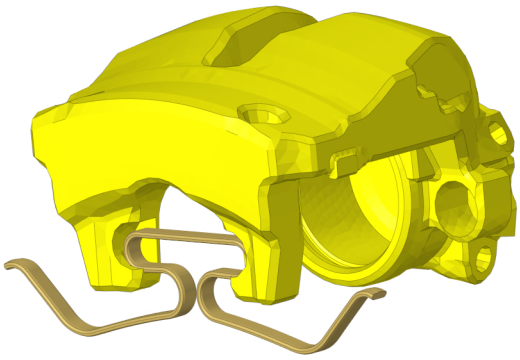

Figure 2.3: Floating caliper housing

2. **Carrier**
   The carrier illustrated in Figure 2.4 is connected to the caliper and it comprises a flange which is positioned parallel to the rotor disc plane. The face of this flange acts as shoulders on respective sides. The back plate assembly of the inboard brake pad is configured to guide the lateral movement of the pad. It also comprises a guide groove for the outboard pad that is held by the caliper. This component is bolted to the wheel hub assembly (also known as the knuckle).

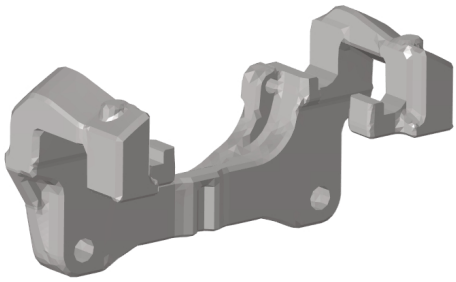

Figure 2.4: Carrier

3. **Friction pads**
   The friction pads are friction materials riveted on a steel back plate, see Figure 2.5. They convert kinetic energy to thermal energy by friction produced while rubbing against the rotor disc. The friction material is a key factor for the performance of the brakes. The outboard friction pad is clamped and held in position between the carrier and the caliper housing with the pretensioned omega spring. The inboard friction pad is riveted to the piston clip and is resting on the caliper housing.

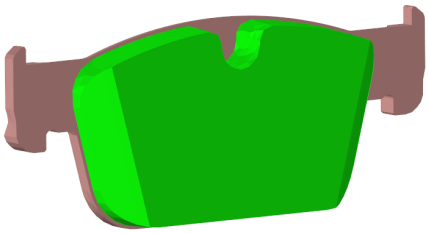

Figure 2.5: Friction pads

4. **Brake disc**
   The brake disc is a rotating circular plate that is mounted on the wheel hub and is sandwiched between the friction pads. The design of the disc in Figure 2.6 is optimised for an average operating temperature of 350 °C with ventilation acting as a heat sink. Types of discs include solid, drilled, slotted/grooved and dimpled designs. The most commonly used design is the ventilated design with two faces of disc spaced apart featuring channels to allow good heat convection that prevents the disc from cracking and enhances the pads life.

Carbon ceramic brakes, though expensive, are a good trade off with high heat resistance, high corrosion resistance and also better aesthetics.

Figure 2.6: Brake disc

5. **Piston rubber seal and dust boot**
   The piston rubber seal with a square cut design is a multi-functional component tightly mounted between the caliper seal groove and the piston which prevents fluid leak to the air side of the caliper. The piston seal deforms when brake force is applied. This retracts the piston and the brake pads away from the disc. The piston roll back is stabilised by the seal. The piston and the seal are protected from any debris or water by a dust boot that is mounted on the caliper illustrated in Figure 2.7.

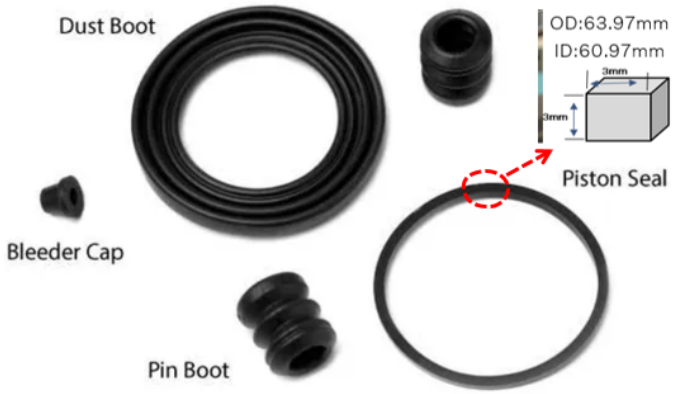

Figure 2.7: Piston rubber seal and dust boot [7]

6. **Piston and piston clip**
   The piston is responsible for the deflection of the pads using the fluid pressure in the hydraulic system. The piston is mounted inside the caliper housing. While sport cars have multiple pistons mounted on both sides of the rotor, most common brake calipers use a single piston to actuate the pads. The

piston clip is a device connecting the friction pad with the piston where one side is press fit into the piston and the other side is riveted to the pad shown in Figure 2.8.

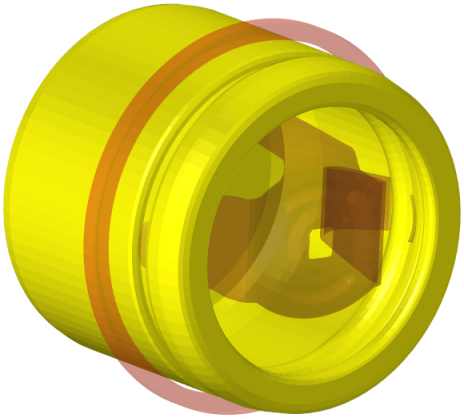

Figure 2.8: Piston and piston clip

2.2.2 Brake drag torque

Residual brake drag torque is a result of pads being in contact with the rotor disc while brake pressure is released, causing residual dynamic friction/resistance to the motion of the wheel. There are several direct and indirect parameters influencing the drag torque out of which few are mentioned in Figure 2.9.

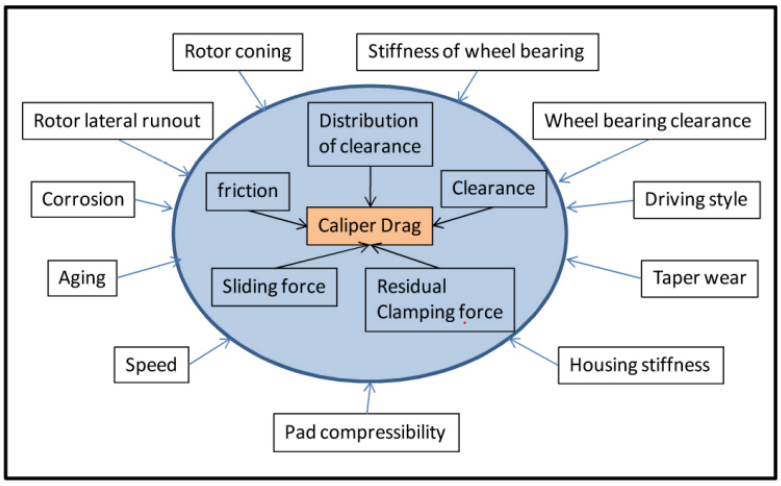

Figure 2.9: Schematic diagram of influences on residual drag torque [8]

- Distribution of clearance
- Clearance
- Residual clamping force
- Sliding force
- Friction

One of the main causes of brake drag is linked to the caliper properties ascertaining the clearance, i.e., either possibly due to the initial gap between pad and disc or by the residual clamping force after applying the brake. Since, the pad is in contact with the disc, the sliding force on pads, the stiffness of the inner lining material, the coefficient of friction between the surfaces and the caliper housing stiffness, are factors that directly have an influence on drag [8].

Indirect parameters that are not linked to caliper properties are rotor coning, lateral run-out, taper wear and pad compressibility.

- Rotor coning is caused by the thermal deformation of the disc in its plane. This means radial expansion which results in bulging outwards, thus increasing thickness of the disc relative to its original disc shape [8].

- The stiffness of the wheel bearing and the clearances between the bearing and the rotor lead to a tilted condition of the rotor which gives rise to lateral run-out that resembles rotor coning in some cases [8].

- Taper wear or uneven wear of the lining material is caused by a less stiff caliper housing which decreases the rigidity of the component causing less clearance between pad and disc [8].

- Pad compressibility is a factor influencing ride comfort (e.g. noise and vibration) and when increased, it leads to decreased clearance gap and hence, results in drag torque [8].

Other factors like aging, corrosion and driving style are also major contributors to drag torque and should be investigated [8].

2.3 Drag knee-point

To illustrate the behavior of drag, a graph of drag torque, measured at a particular rotational speed and the hydraulic brake pressure experienced by the caliper is plotted as shown in the Figure 2.10. The graph shows the outcome of applying brakes up to a specific pressure, later releasing them, and measuring brake drag torque at nominal pressure 0 MPa as depicted in Figure 2.11. The curve in Figure 2.11 shows a "knee-point" where the gradient of the trend line notably changes, which corresponds to a caliper condition for which running clearance no longer exists. Measurements drawn to the left of the drag knee-point reveal caliper drag behavior in areas with running clearance. A seal typically retracts its piston to a regulated position once the hydraulic brake pressure is removed since the caliper deflection at low pressures is quite modest. However, as the hydraulic pressure in the brakes rises, the piston could start to slip through its seal, reducing the running clearance. The relative sliding between the seal and its piston would be subtracted from the original running clearance to determine the new running clearance. Hence, a drag knee-point might be achieved if the running clearance is equal to the relative

sliding distance between a piston and its seal [1].

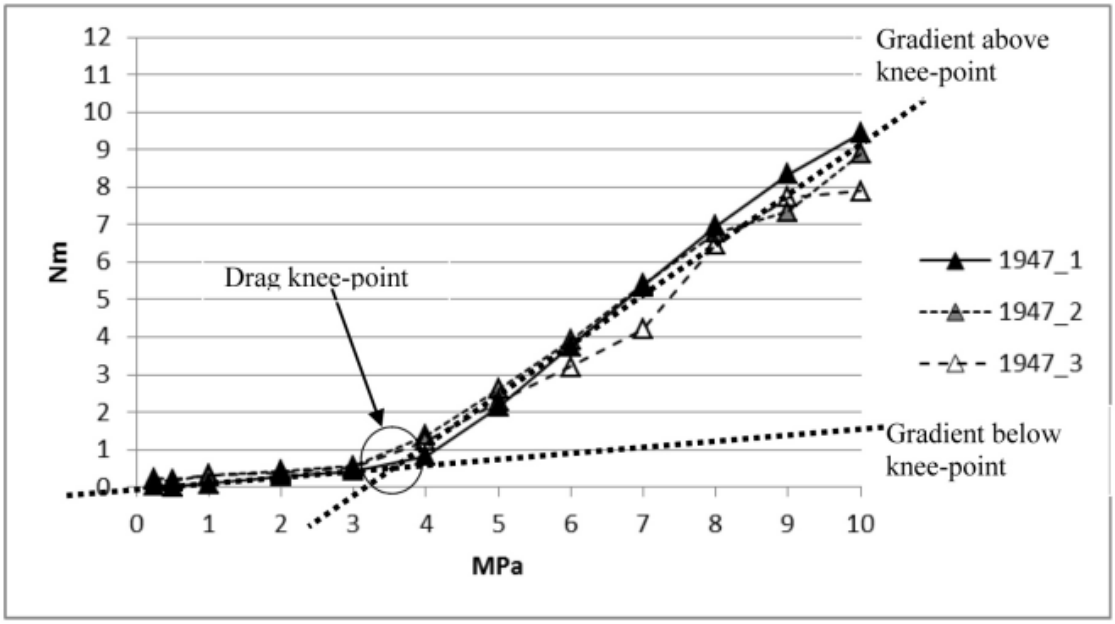

Figure 2.10: Drag knee-point [1].

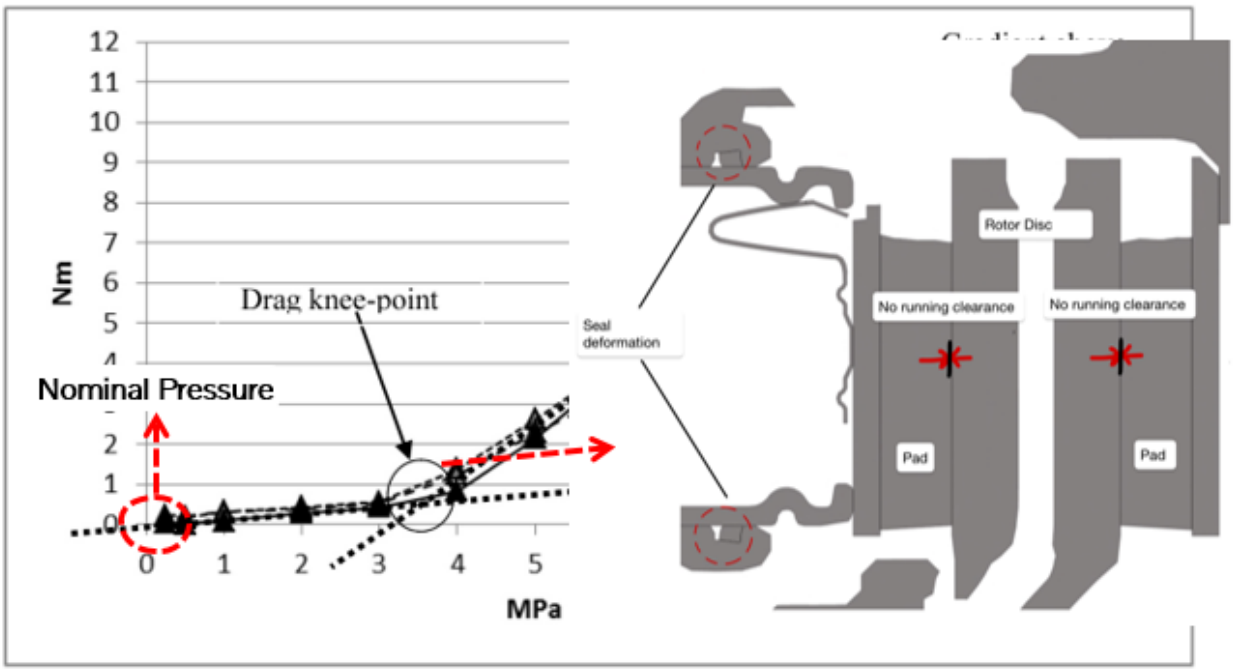

Figure 2.11: Drag knee-point referenced with FE brake assembly model [1].

2.4 Computational contact mechanics

Finite element analysis is a computational numerical method using discretization to solve engineering and mathematical problems. Any complex engineering problem that can be defined using differential equations and boundary conditions can be analysed. In this thesis work, the standard/implicit algorithm in Abaqus is used to perform static simulations.

In implicit analysis, the state of the system at a certain time-step cannot be deduced solely from the state of the system at previous time-steps. Hence, at each time-step, a linear or non-linear system of equations needs to be solved to obtain the state of the system at that time step. This is in contrast to explicit analysis where the state at a certain time step can be obtain solely based on information from previous time steps. [11]

2.4.1 Contact formulation

Contact mechanics study involves either the study of surface interaction between the components or the relative motion between them. The resulting examination of normal forces acting on the bodies is basically the contact force. At a macroscopic level, there is an interaction between bodies at the point of contact resulting in exchange of energy. A shear force is created, if friction between two bodies exists and cause resistance to the sliding motion (or, tangential motion) [10].

A contact problem is categorised as a boundary non-linearity, where body1 has impenetrability with body2. A stiffness relationship between two independent bodies is not defined, resulting in an uncoupled stiffness matrix. Penetration is prevented between two or more sets of bodies defining interaction between the contact elements [10].

Surface-to-surface and node-to-surface discretization are Abqaus specific notions related to contact modelling. The master-slave approach is used by node to surface contact formulation. The slave surface nodes slide over the master-surface element faces in this case. In this contact algorithm master surface nodes can access slave surface nodes. Surface-to-surface contact discretisation is opted to simulate contact conditions. If the surface geometry is reasonably well represented by the contact surfaces, surface-to-surface discretization delivers more accurate stress and pressure results than to the node-to-surface discretization. When compared to enforcing contact criteria at individual slave nodes, the surface-to-surface formulation gives a better result by enforcing them on an average basis across regions surrounding slave nodes. This is because the average regions are roughly centered on slave nodes. Each contact constraint will primarily consider one slave node while also taking into account neighbouring slave nodes. Individual node penetration is possible but huge undiscovered penetrations of master nodes into the slave surface are not possible with this discretization [9].

As an example with dissimilar mesh refinement on the contacting bodies, Figure 2.12 shows contact enforcement for node-to-surface and surface-to-surface contact. The contact direction is determined by the mean of the perpendicular against the slave surface in the slave node's immediate vicinity [9].

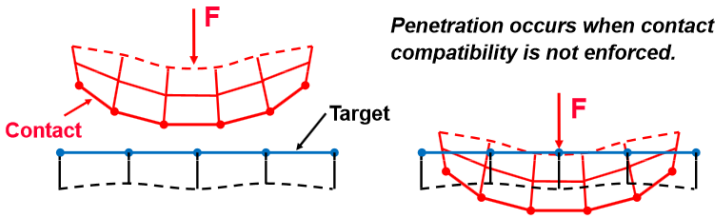

Figure 2.12: Contact surfaces without compatibility [9].

The most general tracking approach is finite-sliding contact, which allows for arbitrary relative separation, sliding, and rotation of the contacting surfaces. The connectivity of the currently active contact constraints changes with relative tangential motion of the contacting surfaces in finite-sliding contact [10].

On enforcing contact compatibility, the interpenetration between the contact system can be prevented. Contact compatibility is driven by a mathematical method named contact formulations using FEM packages. Figure 2.12 depicts penetration, while not enforcing contact compatibility. The penalty function and the Lagrange multipliers method provide the desired solutions to body contact problems. The main distinction between them is how they incorporate the potential energy of contacting surfaces into their formulation [9].

2.4.2 Contact constraint enforcement method - Penalty method

The penalty method approximates the behavior of hard pressure-overclosure method because the contact force is proportional to the penetration distance. In this method, a certain degree of penetration will occur. The penalty method has the following advantages:

- If contact stiffness k_n is too low, the penetration x_p will be too high (can be in the same order of displacement as the penetration distance).
- The numerical softening can mitigate over constraint issues and reduce the number of iterations required in the analysis.
- It can be implemented without using Lagrange multipliers, which improves solver efficiency.

This method includes a penalty term to improve the solving process. The penalty term in contact problems includes the stiffness matrix of the contact surface. The matrix is the result of the idea that one imaginary body penetrates another [9].

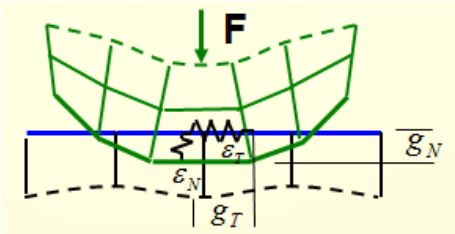

Figure 2.13: Illustration of the penalty method [9].

As depicted in the figure 2.13, pure penalty method is analogous to placing a stiff spring between two parts that must come into contact with each other. In the following equation, when contact stiffness k_n increases for a given contact force (normal), the resulting penetration x_p decreases [9].

$$F_n = k_n * x_p \tag{2.1}$$

If k_n is too high, a small change in x_p results in a large change of contact force F_n or contact pressure, resulting in lack of convergence. The FEA program calculates contact stiffness k_n by default which is based on the size and material properties of the underlying solid element [9].

The penalty method is available in both linear and non-linear variants in Abaqus - Standard. Penalty stiffness can be defined, in the general case, in whatever way the user chooses to specify it. A linear relationship between contact pressure and overclosure, as seen in Figure 2.14, is just one example and not a standard. Comparitive standard of linear and nonlinear pressure-overclosure relationship is depicted in Figure 2.14 .

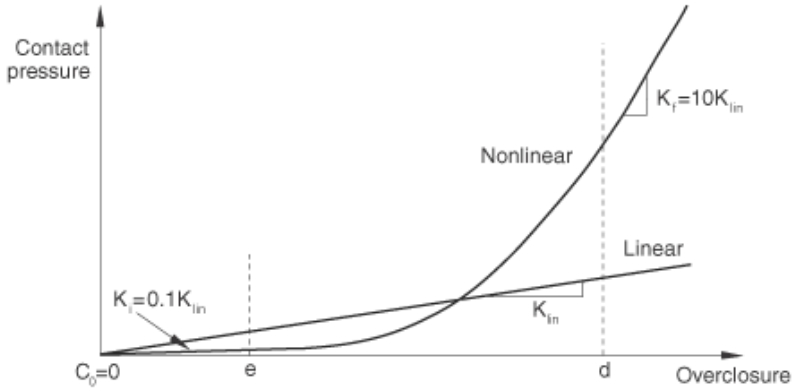

Figure 2.14: Comparison of linear and non-linear pressure - overclosure relationship [12].

Linear penalty method is used in this thesis work where the penalty stiffness is scaled to the underlying element stiffness in the Abaqus-Standard software package. As discussed, in modifying a linear penalty stiffness, one can scale or reassign the penalty stiffness. Contact penetrations caused by the default penalty stiffness have

little effect on the results in most cases. However, these penetrations can occasionally contribute to some degree of stress inaccuracy (for example, with displacement-controlled loading and a coarse mesh). For the finite-sliding, surface-to-surface contact formulation, the linear penalty method is used by default [12].

2.4.3 Pressure-overclosure relationship

The "hard" type of pressure-overclosure (penetration) contact relationship reduces the tensile stress being transferred across the interface by limiting the penetration of the slave surface into the master surface at given constraint locations [13].

Abaqus software package's contact modeling capabilities provide access to a library of "surface constitutive models". The definition of the contact pressure between two surfaces at a point (p), as a function of the surfaces' "overclosure (h)", is part of this library in Abaqus-Standard. The following sections describe hard contact relationship model for $p = p(h)$ [13].

The hard contact relationship is represented numerically as shown below [13]:

$$p = 0 \; for \; h < 0 \text{ (open contact)} \tag{2.2}$$

$$h = 0 \; for \; p > 0 \text{ (closed contact)} \tag{2.3}$$

In a mixed formulation, the contact constraint is enforced with a Lagrange multiplier representing the contact pressure. The contribution to virtual work is represented in the below equation [13]:

$$\delta \prod = \delta p(h) + p\delta h \tag{2.4}$$

The contribution's linearized form is :

$$d\delta \prod = \delta p(dh) + dp(\delta h) \tag{2.5}$$

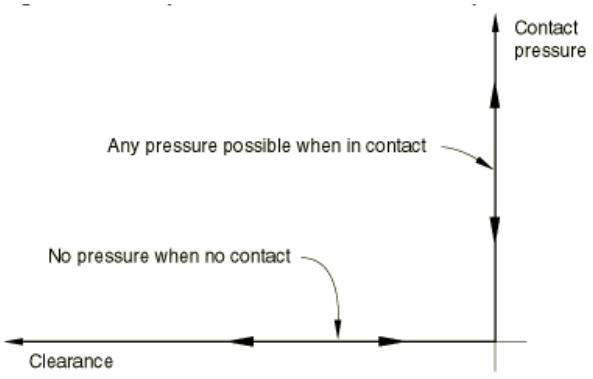

Figure 2.15: Pressure-overclosure relationship [14].

Figure 2.15 depicts the contact pressure-overclosure relationship. The zero-penetration condition may or may not be strictly enforced depending on the constraint enforcement method used by the user. If the contact pressure is reduced to zero, the surfaces

separate. When the clearance between two surfaces becomes zero, they come into contact [14].

2.5 Hyperelastic model

As the name implies, hyperelastic models deal with elastic materials. On application of load, such materials deform and when the load is released, they return to their original shape. Hyperelastic models, in contrast to Hookean elastic models, have a non-linear strain-stress relationship as displayed in Figure 2.16 . It is also referred to as a non-linear material model because large strains can be applied. In this project, modelling the piston seal's material with higher strains and deformed shape. Hyperelastic behaviour modelling is implemented by fitting relevant experimental data to appropriate strain energy density potential models. These hyperelastic models are typically used to model rubber subjected to large strain, as in our case with the rubber seal [15].

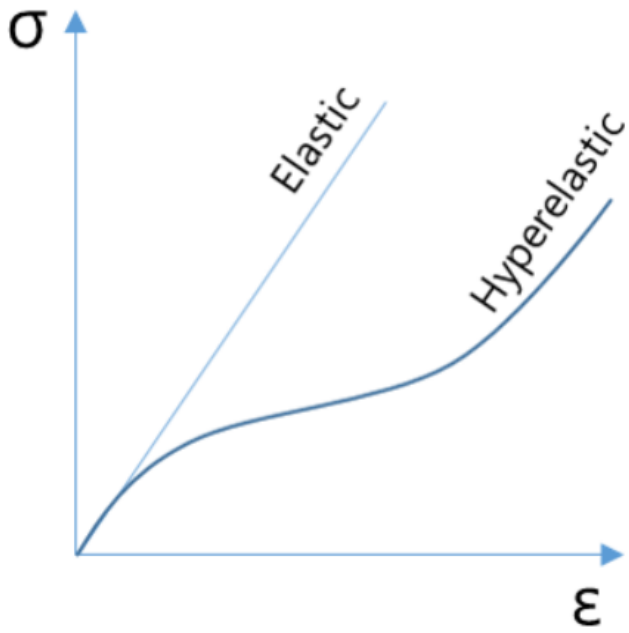

Figure 2.16: Comparision of hyperelastic and linear material.

Abaqus curve fitting procedure accepts the results of the experimental tests shown in the Figure 2.17. By fitting a curve to the test data, discrete stress-strain data points can generate a representative continuous stress-strain curve. By doing this analysis, which is inherent in hyperelastic models, non-linearity is enabled [15].

Outlines of loading condition and deformation for different tests are depicted in Figure 2.17. Real time test data under compression of hyperelastic materials is preferable as specimens undergo deformation modes experiencing higher strain which is not linear [15].

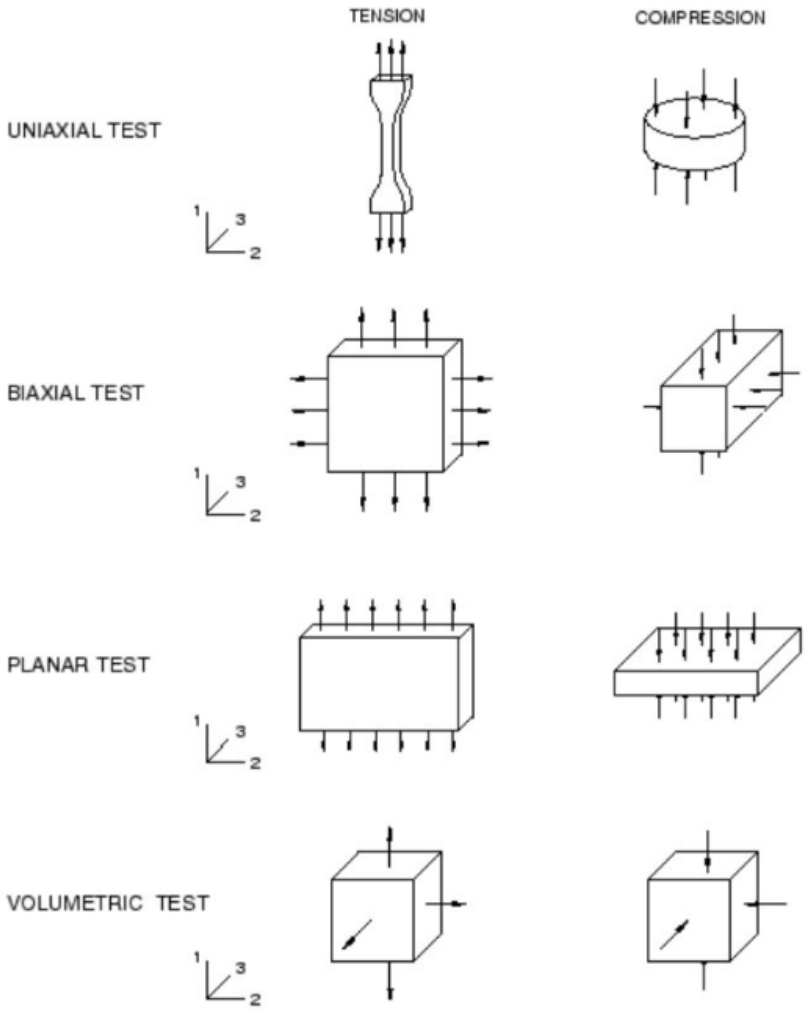

Figure 2.17: Schematic of deformation modes [15].

Strain energy density function equation consists of two terms: deviatoric term that is used to model the shape change behavior and volumetric term that is used to model the volume change of hyperelastic material [16].

$$`U = \underbrace{\sum_{i+j=1}^{N} C_{ij}(\bar{I}_1 - 3)^j}_{Deviatoric\ term} + \underbrace{\sum_{i=1}^{N} \frac{1}{D_i}(J_{el} - 1)^{2i}}_{Volumetric\ term} \tag{2.6}$$

Abaqus provides several variants of the strain energy potential models as listed.

- Polynomial (Moonley, Rivlin, neo-Hookean, Yeoh, reduced polynomial)
- Ogden
- Arruda-Boyce
- Marlow
- Van der Waals

Strain energy potential will introduce various constants (C_{ij}, D_i, N) depending on the selected model (e.g. Polynomial, Marlow, Ogden, etc.) and therefore, will have a distinct final mathematical form. If the availability of data is from multiple experimental tests (minimum uniaxial and equibiaxial test data), then Ogden and Van der Waals forms better fit the results. If limited test data is available, then either Arruda-Boyce, Van der Waals, Yeoh, or reduced polynomial forms demonstrate acceptable behavior. While only one set of test data (uniaxial, equibiaxial, or planar test data) is accessible, the Marlow form is preferred. The equivalent deformation modes are displayed by tests for in-compressible material and hence the results obtained are equivalent to each other as listed below [16]:

- Uniaxial tension $\longleftrightarrow$ Equibiaxial compression.
- Uniaxial compression $\longleftrightarrow$ Equibiaxial tension.
- Planar tension $\longleftrightarrow$ Planar compression.

3
Approach and Implementation

This chapter summarises the approach of using the FE program Abaqus to validate brake drag torque mechanisms on a qualitative and quantitative level. Firstly, an augmented simplified piston-caliper housing and a piston seal were modelled and validated to quantify and simulate the roll-back mechanism caused by the seal. Next, an adapted version of an available detailed NVH friction brake assembly FE model was established by adding new components that made it compatible for drag analysis. The baseline NVH model did not include clearances of rubber seal, piston clip and omega spring. These components were added, as they have a major contribution to the stiffness of the assembly. Later, loading and unloading simulations were run on the augmented model.

Qualitative FE simulations of the augmented model offered an approach to analyse and define mechanisms in the complete friction brake assembly model. This allowed for implementation of the rubber hyperelastic material. The hyperelastic material data obtained through experimental tests were implemented into the rubber seal model using Marlow's method in Abaqus. Boundary conditions and contacts were later defined for the complete model to validate non-conservative forces in the system which were verified by the deformations. This FE model was used to simulate for static conditions which were correlated to braking pressure response on a real braking system. These validated model results mimic brake drag as a function of the brake pressure (drag knee-point). Finally, a parametric study to comprehend the influence of various components contributing to brake drag was carried out. An overview of the process steps in the project is mapped in the workflow diagram in Figure 2.17.

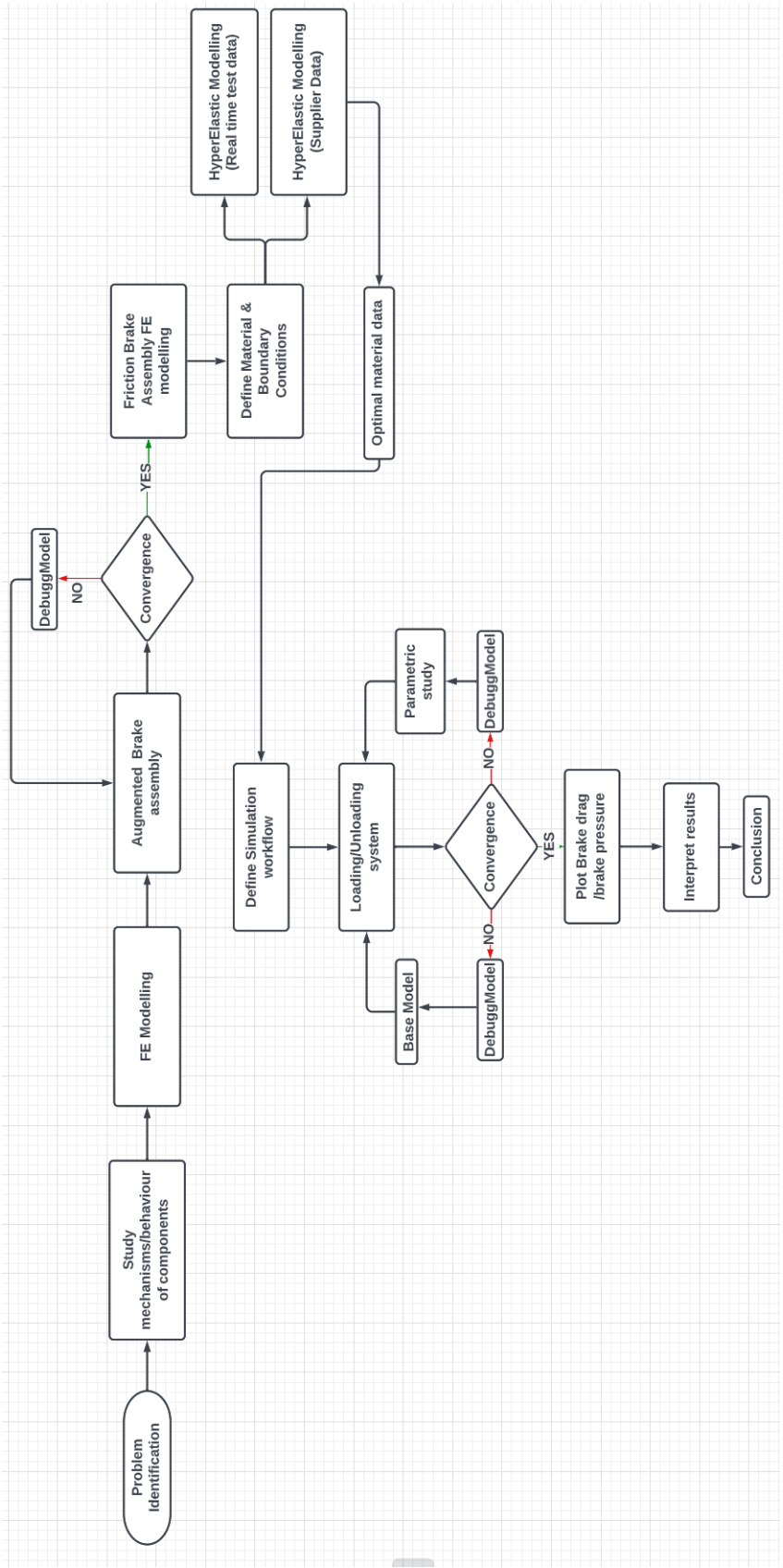

Figure 3.1: Project workflow chart

3.1 Augmented FE model

The motive to build an augmented model was to quantify factors influencing the brake drag for a simple system. This requires less computational time and convergence issues can be resolved faster. On completing the FE modelling of the system, the simulation work flow is determined to correlate with realistic boundary conditions as depicted in Figure 3.2.

Retraction mechanism of the seal was an intriguing behavioural study necessary in the project to calculate the drag torque, as it plays a major role in pulling back the piston to its original position. So, a minimalist system containing the rubber seal, lining material and an integrated model of the housing and the rotor disc was modelled, see Figure 3.2.

The FE model was meshed with 3D hexahedron elements for all components. These elements have a high degree of accuracy and can easily be used to model less complicated geometry. The material modelling of components is carried out by defining physical properties (Youngs modulus, Poisson's ratio and density) of the piston, lining stiffness and caliper housing. These are modelled as steel whereas the seal is assigned with rubber having an elastic modulus of 20 MPa and Poisson's ratio of 0.3. The undeformed diameter of the rubber seal is larger than the caliper housing. Hence interference fit modelling (shrink fit) is used to compress the rubber seal between the caliper housing and the piston. In the first load step, rubber seal wall contacts are initialised using shrink fit as shown in Figure 3.3. The boundary conditions are defined by constraining the piston and the caliper housing in all DOFs. In the next load step, as illustrated in Figure 3.4, the load is applied along the lateral direction of the piston. This force tends to push the lining material to the wall of the caliper housing deforming the seal along the same direction. Lastly, the applied lateral load is removed in a "release lateral load step", where the deformed seal retracts the piston to its original position with negative pressure created on the piston. Also, the boundary conditions were defined as in the previous load step but with one particular change, i.e., zero load applied on the piston. In this condition, the elasticity of the deformed rubber, see Figure 3.5, mimics the mechanism.

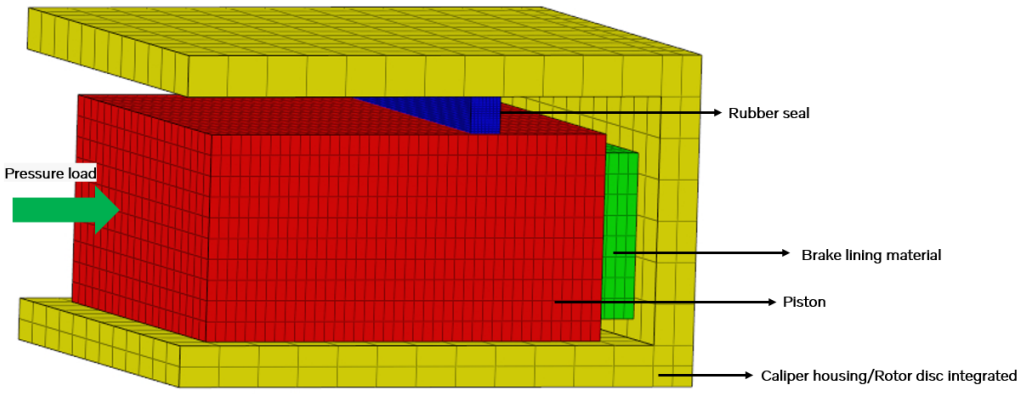

Figure 3.2: Augmented finite element model

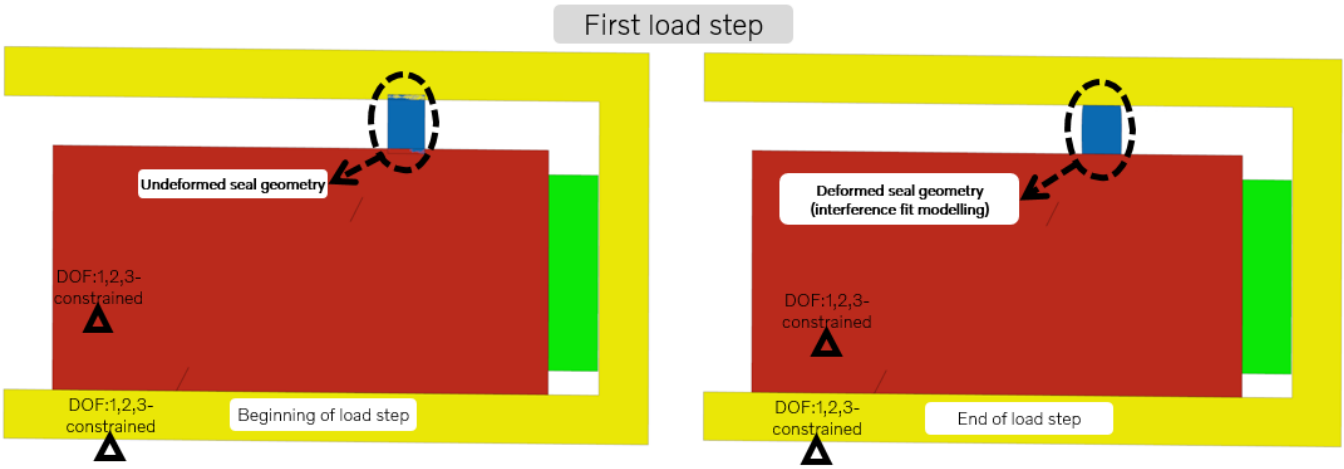

Figure 3.3: First loadstep

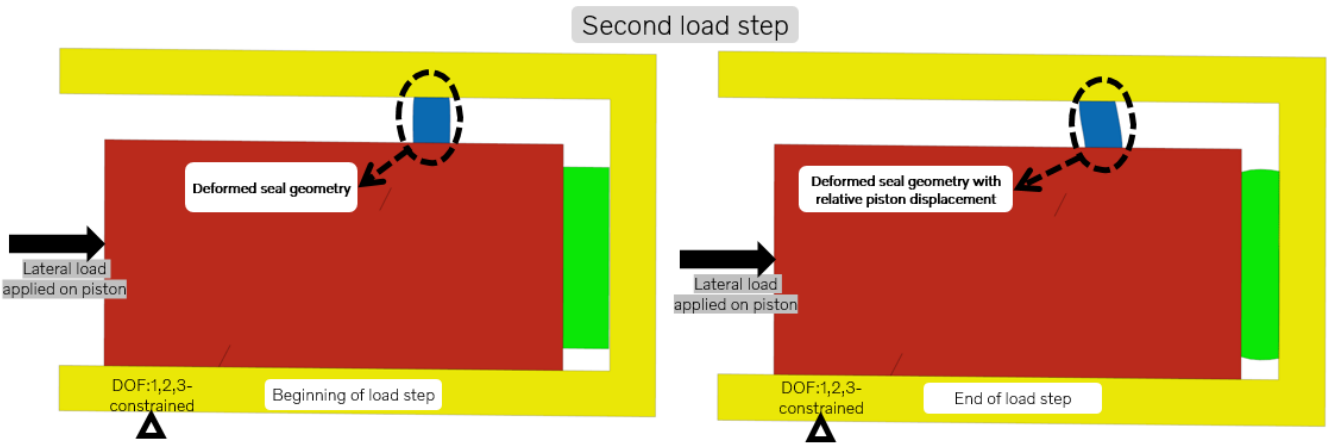

Figure 3.4: Second loadstep

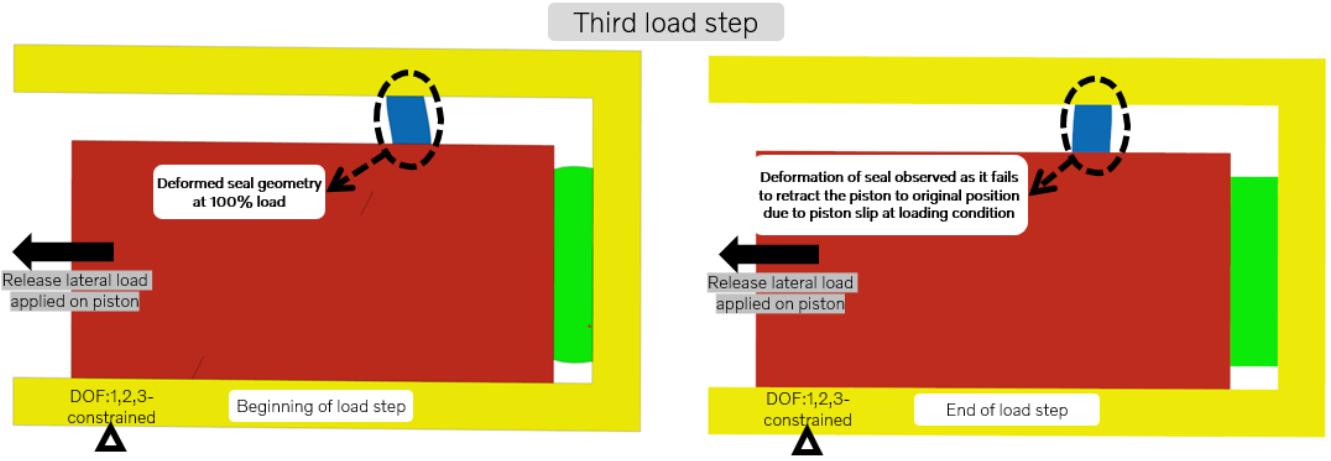

Figure 3.5: Third loadstep

As observed in Figure 3.6 while analysing simulation results there is a piston slip over the rubber seal. This piston slip reduces the running clearance as the relative displacement of the piston to seal is not small. At 80% of load it is observed that the relative displacement of piston to seal has drastically increased, as shown in Figure 3.7, leading to a drag knee-point. The running clearance at the drag knee-point is changed over the original running clearance causing brake drag. This augmented model fortified the methodology to define the mechanism of seal compression, seal retraction and boundary conditions which was used for implementation in the brake assembly.

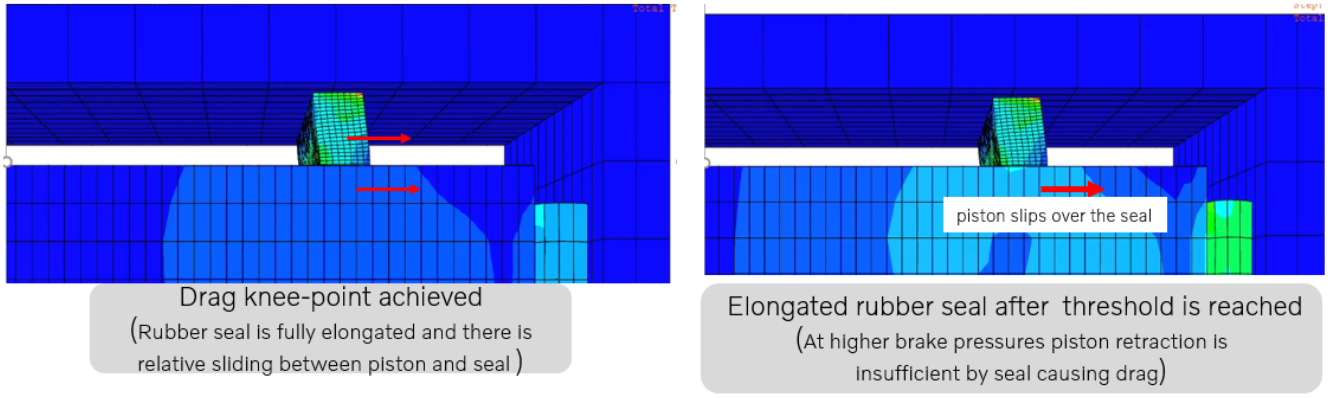

Figure 3.6: Simulation results using augmented model

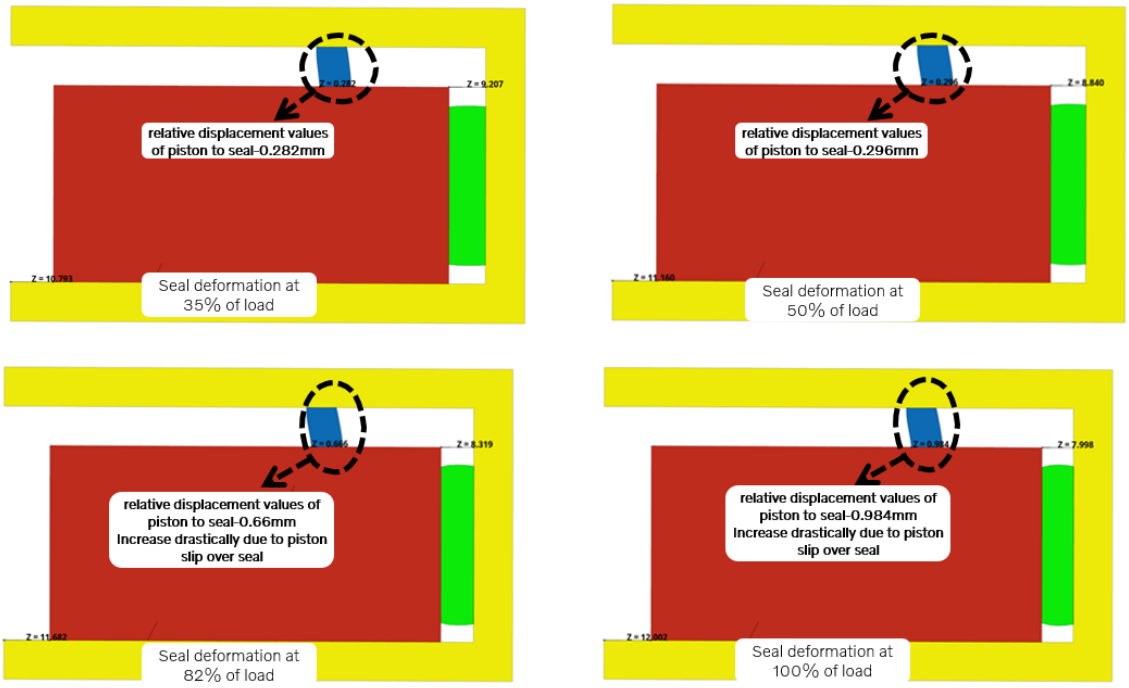

Figure 3.7: Overview of relative displacement of piston to seal at different loads

3.2 Hyperelastic model with physical test data

Augmented model analysis interpreted the importance of rubber seal behaviour. Hence, the physical property of the seal is very significant to optimise and represent hyperelastic behaviour in the simulations. Further, to investigate the residual pressure present in the friction pad and to model the drag characteristics of the seal using hyperelastic property data, experimental tests were performed to measure the static and dynamic stiffness of a rubber seal in compression.

As discussed previously, to obtain Marlow strain energy potential model constants, Abaqus requires one data set of uni-axial stress-strain (either tension or compression) data from a rubber seal specimen. Using this output, hyperelastic properties of the rubber seal is predicted in FEM. In this experiment, a standard uni-axial testing rig was utilised to perform compression test on a specimen mounted as displayed in Figure 3.8.

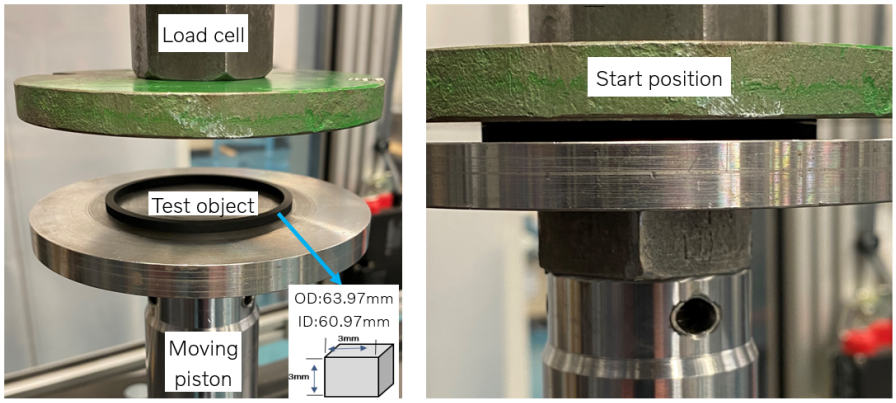

Figure 3.8: Uniaxial compression test setup

The dimensions of the test specimen shown in Figure 3.8 are as follows. The inner and outer diameter is 60.97 mm and 63.97 mm, respectively, along with a thickness of 3.0 mm. Static measurement tests were carried out with and without pre-cycle, as it is a common practise to pre-cycle the rubber material three times with about 110% of the amplitude. The specifications for static and dynamic measurements are :

- Static compression without pre-cycle ranging from 0 - 20% is proportional to 0 - 0.66 mm of the available 3 mm thick rubber seal. Tests are carried out for 5%, 10% and 15% compression. The seal is compressed from 0 - 20% of its original thickness, and the force-compression curve is registered.
- Static compression with pre-cycle ranging from 0 - 20% is proportional to 0 - 0.66 mm of the available 3 mm thick rubber seal. Tests are carried out for 5%, 10% and 15% compression.
- Dynamic compression measurements are carried out by loading the seal at a static 20% compression, superimposed by amplitudes of ± 0.05 mm, ± 0.1 mm and ± 0.25 mm for 0, 1 and 5 Hz frequencies .

Results of rubber seal compression tests, i.e., axial load and axial displacement were converted to stress/strain values. These values were incorporated in Abaqus software to obtain strain energy potential constants for hyperelastic material model by the Marlow method.

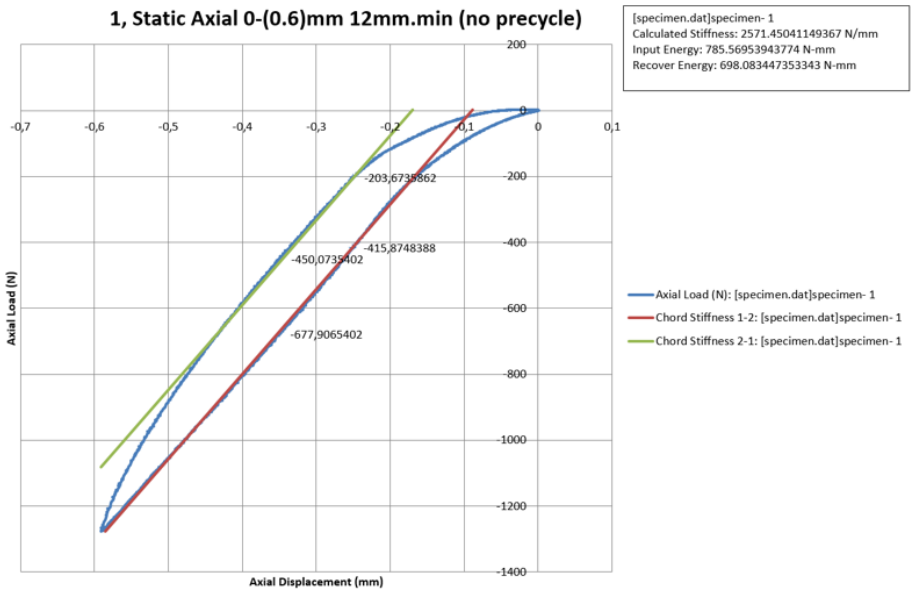

Figure 3.9: Results of uniaxial compression test

3.3 Defining boundary & loading conditions

The existing detailed NVH FE model of the friction brake assembly had to be adapted to carry out the drag simulations. The seal, piston clip and omega spring models were introduced to have a descriptive model of the brake assembly. The NVH model lacked detailing of clearances of rubber seal, omega spring and piston clip. Since these components influenced drag they were incorporated. The rubber seal was modelled with 3D hexahedron elements having a fine mesh of size 0.25 mm to achieve accurate results. The seal node was transformed to a local cylindrical coordinate system using "transform function" in Abaqus. This association of the local system to all nodes facilitate the complete list of input data for boundary conditions of displacement, rotation, concentrated forces and moments to be transformed accordingly. The element data, outputs, contacts, properties, dynamic parameters and materials of individual components were structured as respective input files making it easy to modify these independently.

3.3.1 Contacts definition

A surface-to-surface contact definition was used for modelling of interaction between specific surfaces in the assembly illustrated in Figures 3.10, 3.11, 3.12. As listed in the table below, the surfaces were characterised based on friction and tie contact. Additional parameters like constraint enforcement, pressure-over closure method and surface smoothing were used. "Penalty method- linear" type was used to enable

a smoother convergence and minimal amount of penetration by approximating the hard contact. Surface smoothing was implemented to reduce discretization error with faceted representation of curved surfaces. This also compensated the accurate contact stresses with a relative coarse mesh. Illustration of contacts in the assembly are shown in Table 3.1.

Friction Contact			
Surfaces (element-based)	**Constraint Enforcement**	**Pressure-Overclosure formulation**	**Friction Coefficient**
Piston-Piston Clip	Penalty: Linear	Hard	0.2
Backplate-Piston	Penalty: Linear	Hard	0.2
Disc-Friction lining	Penalty: Linear	Hard	0.4
Caliper Housing-Backplate	Penalty: Linear	Hard	0.2
Carrier-Backplate	Penalty: Linear	Hard	0.2
Carrier-Omega	Penalty: Linear	Hard	0.2
Caliper Housing-Seal	Penalty: Linear	Hard	0
Piston-Seal	Penalty: Linear	Hard	0
Caliper Housing-Piston	-	Tabular	0
Tie Contact			
Inner Backplate- Piston Clip			
Inner Backplate- Inner Friction Lining			
Outer Backplate- Outer Friction Lining			

Table 3.1: Contact definition matrix.

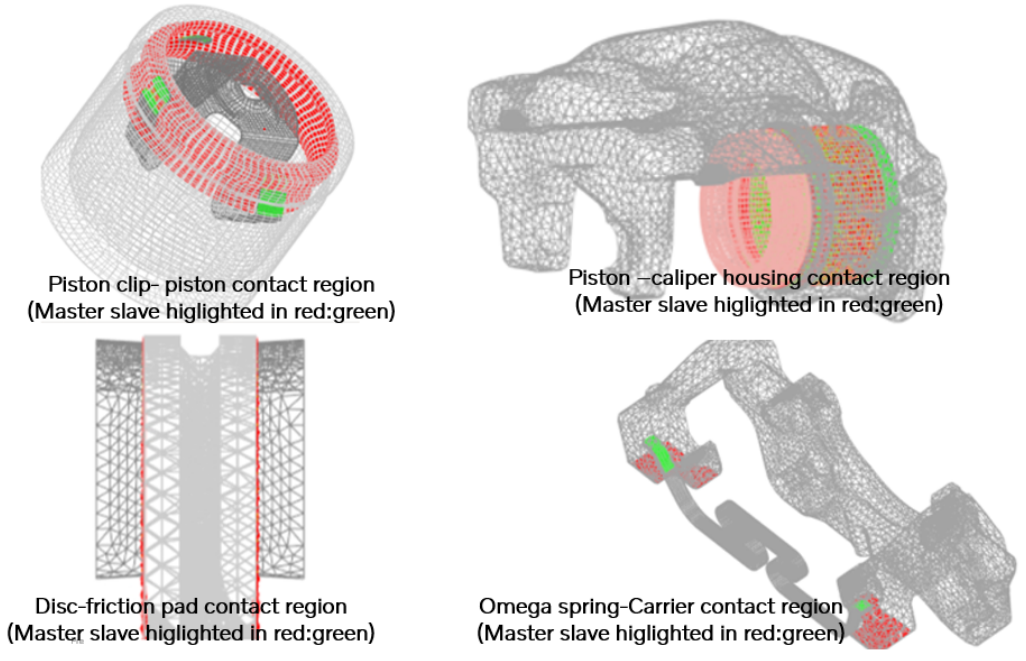

Figure 3.10: Contact illustration

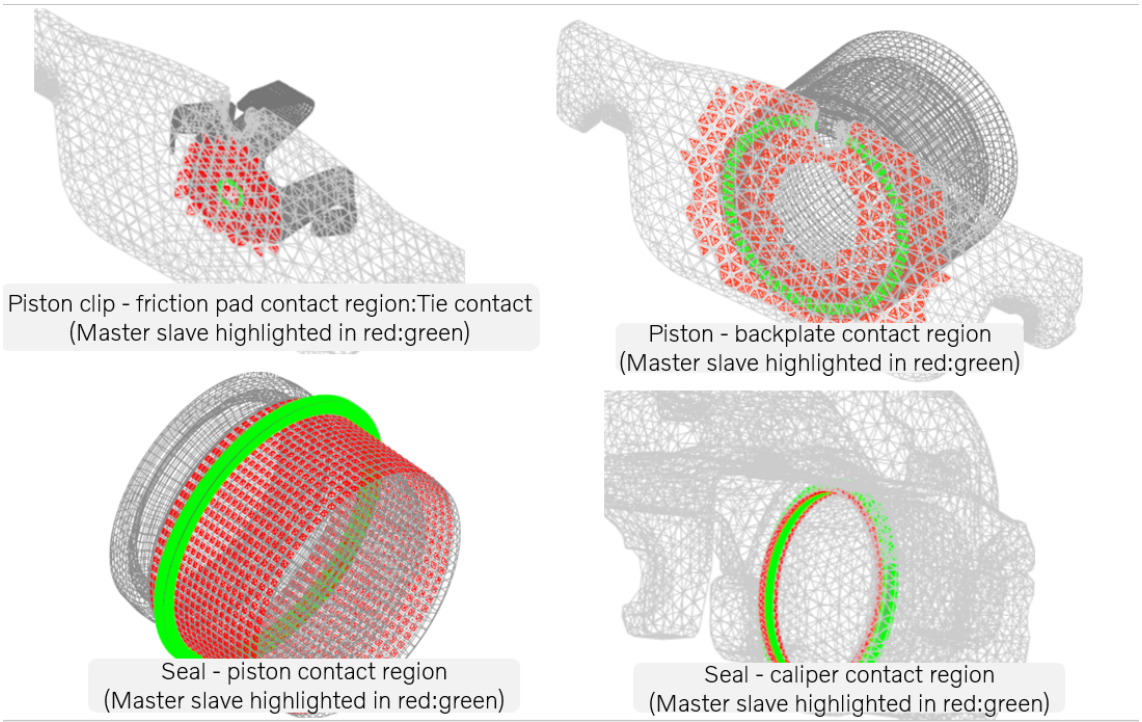

Figure 3.11: Contact illustration

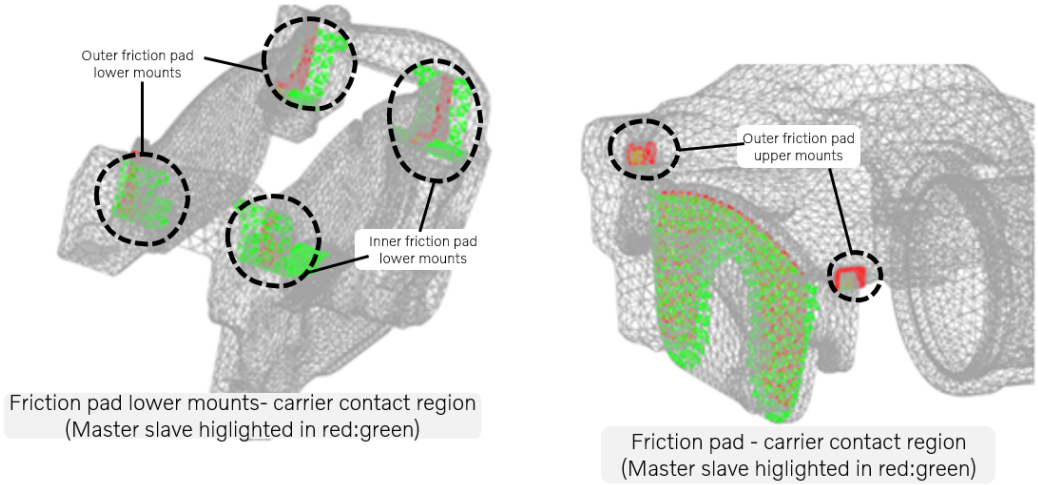

Figure 3.12: Contact illustration

3.3.2 Simulation workflow

In contact simulation, the static instabilities were prevented by intervention approach and hence, a special analysis sequencing was performed.Hence the simulation was divided into several parts to facilitate the convergence caused by static instabilities as in Figure 3.13. Static instable rigid modes are observed if the simulations lack initial contact or gaps closure causing convergence issues, which were counteracted by prescribed displacements enabling convergence.

Figure 3.13: Simulation work flow

Static instabilities are caused by unconstrained rigid body modes and geometric and material instabilities. Based on this, viable options were chosen to carryout analyses.

Three major steps were sequenced as listed below.

1. **Pretension**: Mounting rubber seal, piston clip and omega spring into the system, which involves large overclosure, is necessary to relate to a real brake assembly. In the first step piston clip, rubber seal and omega spring with the local deformation forces were incorporated into the assembly.

   Piston clip, as discussed in the theory, see Section 2.2.1, holds the piston with a snap fit mechanism. This mechanism was defined by applying prescribed displacements on the 3 arms of the piston clip. "Nset" for each node on 3 arms were created and positioned by displacing along the 3 transitional axis and constraining along the 3 rotational axes. Then, the omega spring arms were pretensioned with prescribed displacement along the vertical axis to achieve contact with the carrier. Similarly, the positioning of seals in the caliper cavity was achieved by prescribed displacement of its lower surface. To prevent convergence issues and also while introducing pretension, by using the function "*MODEL CHANGE:Remove", some of the contact pairs were tentatively removed.

   In the second step of pretension, seal contact was introduced while retaining the previous boundary conditions. Since the seal is a hyperelastic model and the instability of the model had to be reduced, only caliper-seal contact was introduced using "*MODEL CHANGE: ADD". The simulation was stabilised using "*CONTACT CONTROL,Stabilize" function in Abaqus. This function introduced weak spring elements with artificial damping factor to aid convergence.

   In the third step of pretension, gradually clip and omega spring contacts were defined to aid static stability in the model. These prerequisite setups were ready to simulate the loading conditions.

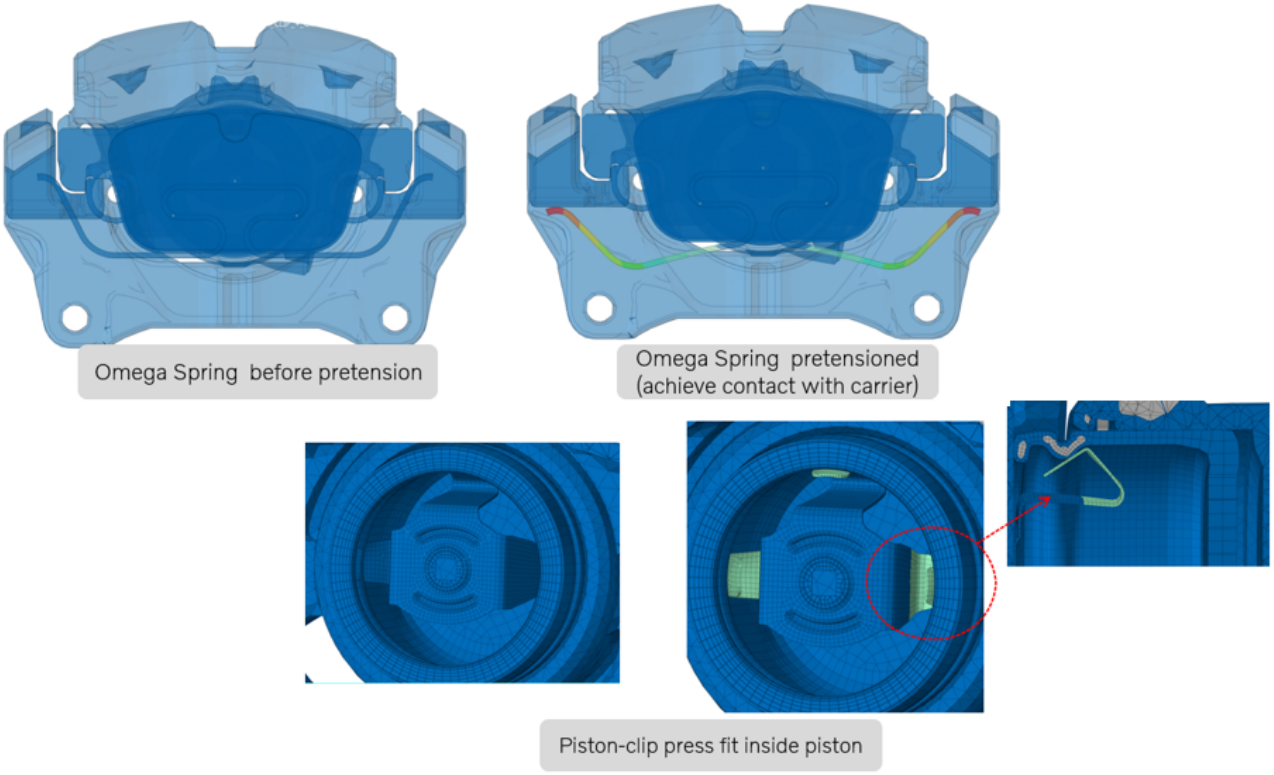

Figure 3.14: Illustration of omega spring and piston clip deformation

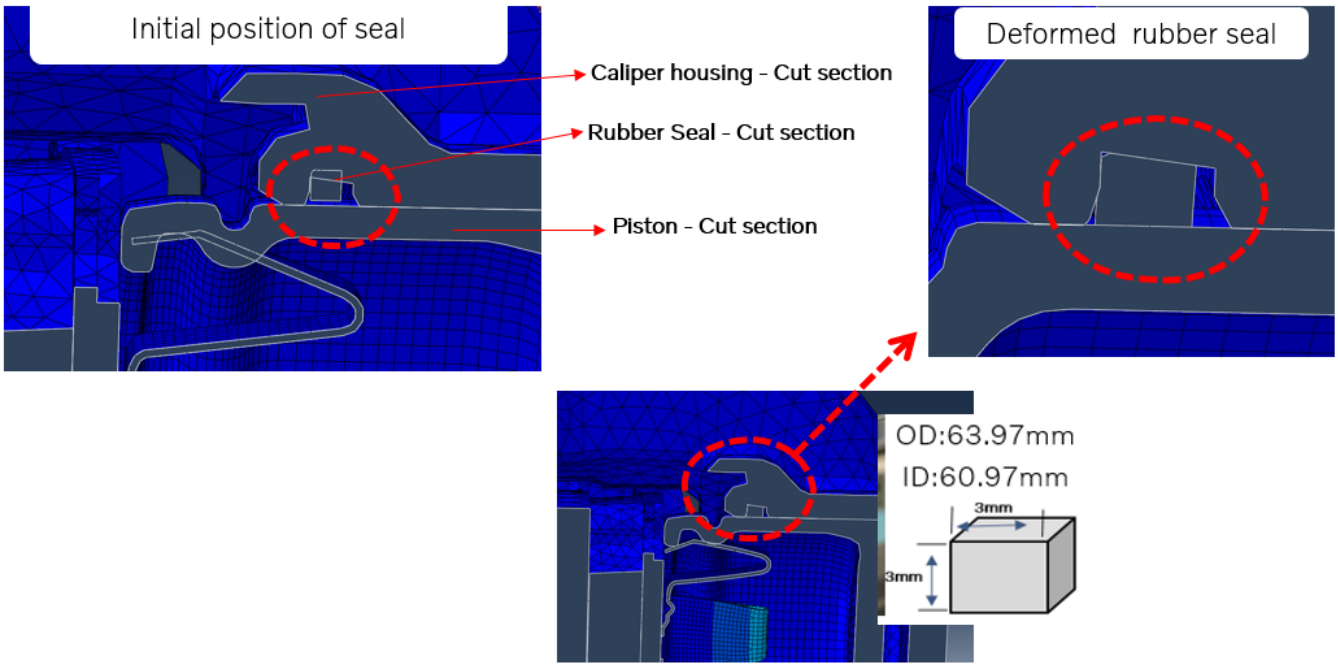

Figure 3.15: Illustration of seal deformation

2. **Apply brake pressure**: As the brake assembly constitutes of an unconstrained rigid mode based on the gap between the friction pad and rotor, it had to be adjusted by displacement controlled loading. Hence the pad contact was initiated by applying lateral displacement to the friction pads towards the rotor while arresting the carrier and rotor disc displacement. Static instabilities were predicted to increase with application of brake pressure.

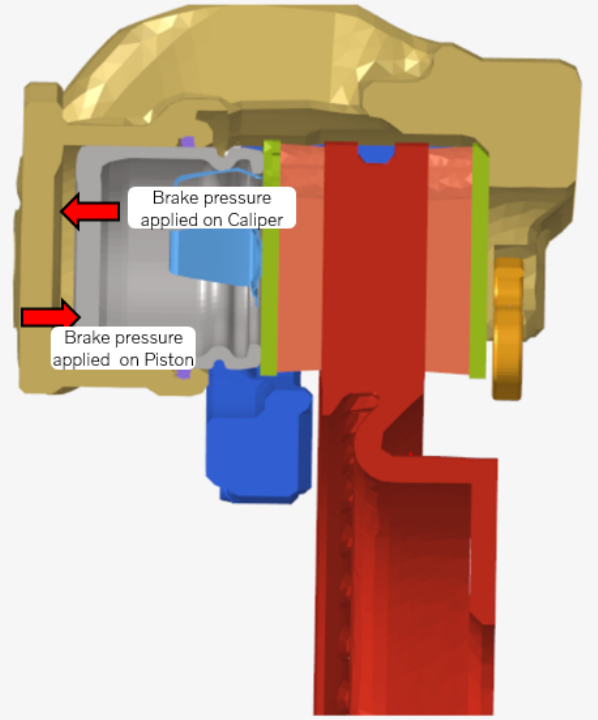

Figure 3.16: Brake force on friction brake assembly

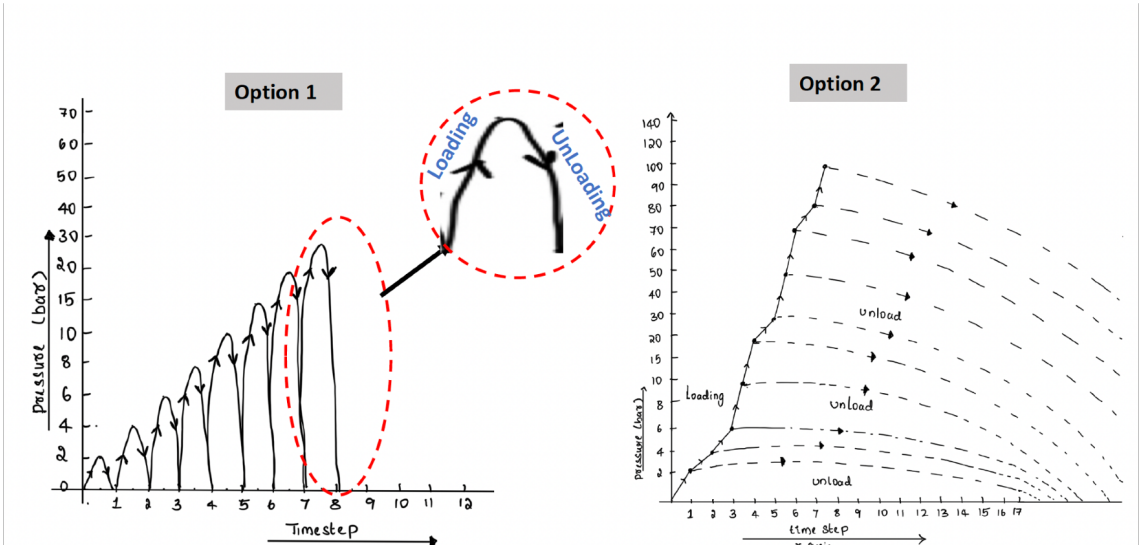

Figure 3.17: Plot illustrating loading and unloading conditions

Two methods were used to load and unload the pads. The first one was to apply and release brake pressure on caliper and piston in consecutive load steps as shown in Figure 3.17. However, achieving contacts by this method was not a viable option with higher brake pressures. Hence, an alternative method shown was to add concentrated force that is equivalent to the brake forces on the piston and the caliper surfaces as illustrated in the Figure 3.16. The boundary conditions for the assembly was given by constraining all DOFs on the carrier bolting point to the knuckle and the rotor mountings to the wheel hub. The brake pressure was varied from 2 bar to 140 bar.

3. **Release brake pressure**: On loading the brakes sequentially increase brake pressure from 2 bar to 120 bar, unloading of brake pressure was carried out. The boundary conditions on the system was similar to the previous step with zero force acting on the caliper housing and the piston.

3.4 Parametric study of factors influencing drag torque

A parametric study was conducted to investigate the influence of longitudinal stiffness of caliper housing and friction pad lining on the brake assembly components causing brake drag torque as discussed in the earlier section. A study of the influence of the omega spring was also carried out as a decrease in its stiffness influences the longitudinal stiffness of seal and caliper. This was achieved by modifying the caliper and lining material stiffness. The observations from the base model displayed a lateral displacement by the omega spring pressing the backplate and the friction pad. Pretension in the contact interface between backplate and carrier as well as backplate and caliper is provided by the omega spring. This behaviour of the omega spring was taken into consideration by varying its stiffness (i.e., youngs modulus). As illustrated in Table 3.2 the range of parameter values were selected to perform the analysis. This ±50% variation was chosen to give a broader approach. Simulations were carried out with the baseline model boundary conditions and pressure loads. Later the validated results were plotted in a graph depicting generic behaviour of the modified brake assembly.

PAREMETER:STIFFNESS	RANGE
Caliper Housing Youngs modulus	±50 % (Increased & decreased)
Friction Pad Lining Youngs modulus	±50 % (Increased & decreased)
Omega spring Young modulus	50% (Decreased)

Table 3.2: Matrix for parametric study of stiffness

4
Results

Section 4.1 outlines the results from the simulations on the brake assembly with the base design material properties exhibiting mechanisms that are similar to a real brake, aiding an accurate model to quantify the drag. In Section 4.2, the results of the parametric study is discussed which incorporates the effect of caliper housing stiffness, effect of friction pad stiffness and effect of omega spring stiffness. Additionally, a comparative study was carried out to validate the baseline model with the parametric study.

4.1 Residual brake torque analysis - Baseline model

The simulations were performed on the baseline brake assembly and the observed generic behaviour of drag torque was plotted as a function of the brake pressure. This is illustrated in Figure 4.1, where yellow line indicates the outer friction pad trend and the grey line signifies the inner friction pad trend.

In these simulations the rotation of the disc was not considered, so the residual forces were converted to drag as discussed. The normal/clamping force that compresses each brake pad against the disc is denoted as F_{normal} and the tangential frictional force acting between the brake pads and disc is designated as F_{residual}. Equation 4.1 illustrates the relationship between the residual forces and normal forces acting on the brake pad.

$$F_{\text{residual}} = \mu * F_{\text{normal}} \tag{4.1}$$

$$T_{\text{drag}} = F_{\text{residual}} * R_{\text{effective}} \tag{4.2}$$

As seen, for low brake pressures (0-20 bar), the drag is first assuming a steeply increasing trend. This is because the simulation assumes that both pads are initially separated from the disc by a clearance of 0.2 mm. In reality, the very first brake application of the caliper will close this gap, at least on the outboard side. Therefore, in actual measurements of drag vs pressure, this steep increase in drag is not observed. In the range of 20-100 bar of brake pressure constant residual torque of 1.8Nm as the initial clearances disappears after 20 bar. In this region the displacement of rubber seal and the piston is equal displaying constant drag torques along these brake pressures. The impact of adjacent component stiffness along this pressure range is minimal. However, at high pressures, i.e., after 100 bar the deformation of these component will cause drag torque, see Figure 4.1. The increase in

drag torque with increasing pressure is observed to be due to piston slip over the seal, where the original displacement is increased. This larger displacement in piston is hard to follow by the seal and retract the piston leading to no running clearance causing increase in drag torque.

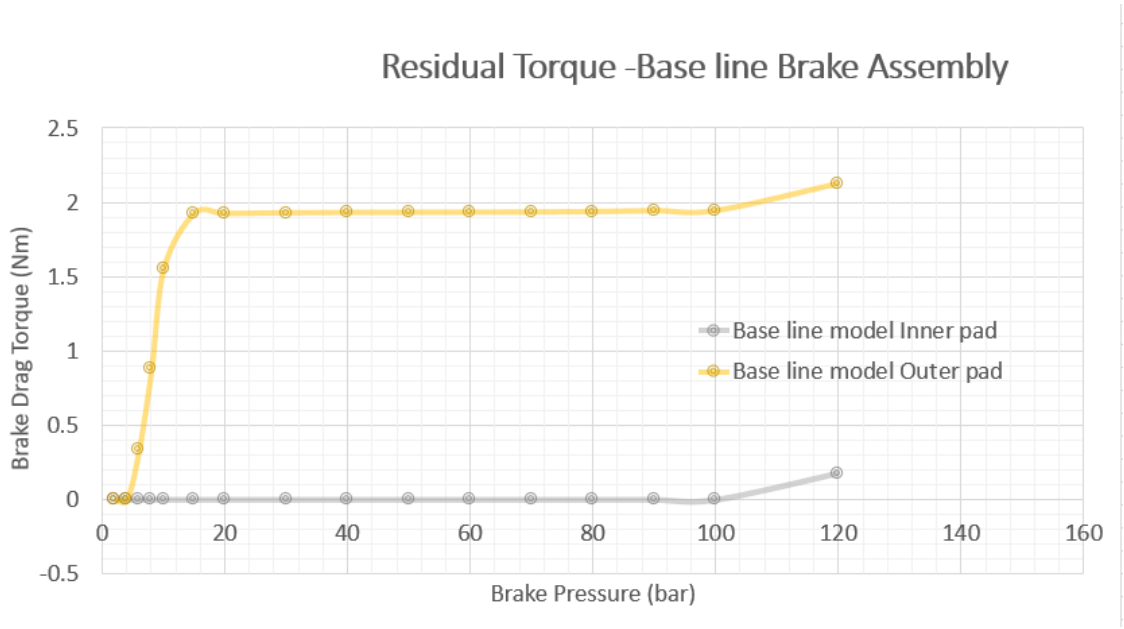

Figure 4.1: Simulation results for baseline brake assembly

From Figure 4.1 it is evident that the drag knee-point occurs at 100 bar of pressure. Additionally, it is noticeable that the trend is similar to the discussions in Section 2.3 corresponding to no running clearance in the model. The FE model was utilized to verify the running clearance of friction pad and disc. The relative displacement of the piston seal to the piston was analysed to study its relation at lower and higher brake pressures. It is noted in Figure 4.1 that at higher pressure, i.e., after the drag knee-point, the displacement between piston seal and piston is not equal causing no running clearance between the friction pads and disc.

Note: Due to FE model convergence issues at higher brake pressure, simulations were carried out only up to 120 bar.

4.2 Results of parametric study of factors influencing drag torque

4.2.1 Effect of caliper housing stiffness

A drastic change is observed in the residual torque in the pressure range of 0-15 bar. This change can be accredited to the simulation initiation with a clearance between pads and disc and similar trends are observed in Section 4.1. The behaviour of the curve remains similar to the baseline model until 100 bars. However, as the pressure values increase, longitudinal stiffness dominates the drag knee-point demonstrated in Figure 4.2. Inner and outer pad drag torque values are referenced in Table 4.1.

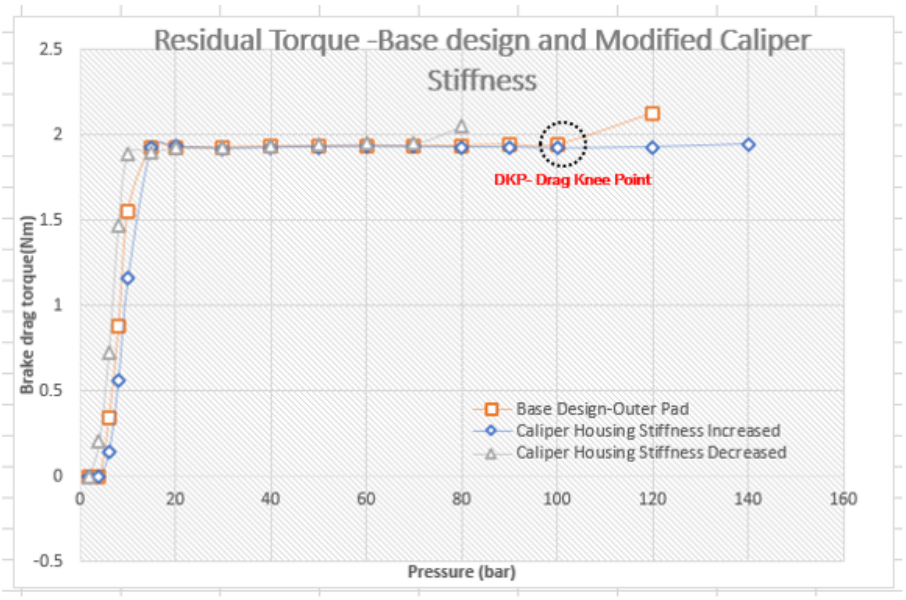

Figure 4.2: Simulation results for modified caliper housing stiffness compared to baseline model

BRAKE PRESSURE (bar)	BASELINE MODEL (Drag Torque-Nm)		INCREASED CALIPER HOUSING STIFFNESS (Drag Torque-Nm)		DECREASED CALIPER HOUSING STIFFNESS (Drag Torque-Nm)	
	Inner pad	Outer pad	Inner pad	Outer pad	Inner pad	Outer pad
2	0	0	0	0	0	0
4	0	0	0	0	0	0.202
6	0	0.339	0	0.141	0	0.723
8	0	0.877	0	0.558	0	1.473
10	0	1.554	0	1.156	0	1.887
15	0	1.924	0	1.925	0	1.901
20	0	1.922	0	1.931	0	1.924
30	0	1.927	0	1.920	0	1.924
40	0	1.929	0	1.926	0	1.936
50	0	1.930	0	1.929	0	1.941
60	0	1.931	0	1.932	0	1.947
70	0	1.932	0	1.930	0	1.948
80	0	1.935	0	1.927	0.087	2.051
90	0	1.941	0	1.928	Convergence Issue	Convergence Issue
100	0	1.942	0	1.921	Convergence Issue	Convergence Issue
120	0.177	2.124	0	1.928	Convergence Issue	Convergence Issue
140	Convergence Issue	Convergence Issue	0	1.945	Convergence Issue	Convergence Issue

Table 4.1: Brake drag torque for modified caliper housing stiffness compared to baseline model

4.2.2 Effect of friction pad stiffness

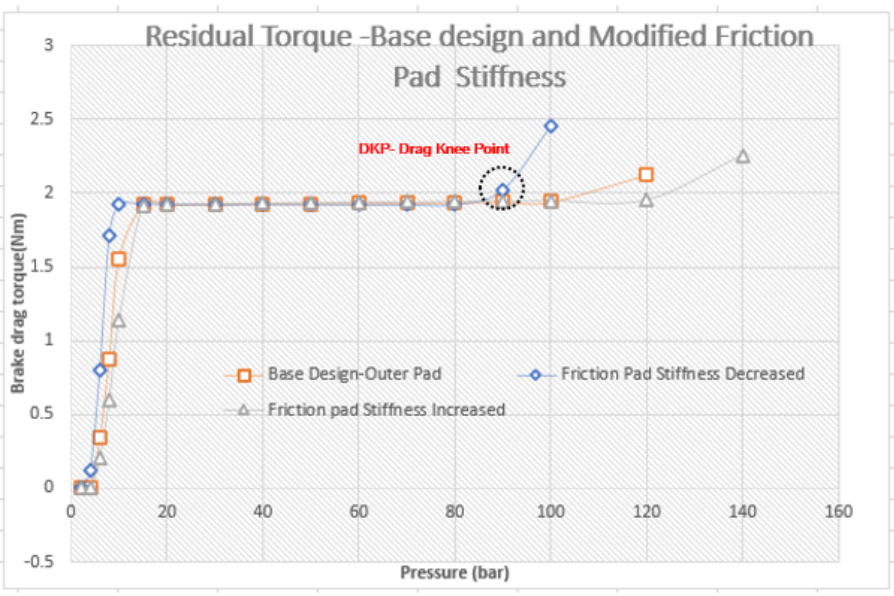

Figure 4.3: Simulation results for modified friction pad stiffness compared to baseline model

In case of the friction pad stiffness, the behaviour of the curve is indistinguishable from the baseline model until 85 bar. Nonetheless, lowering the friction pad stiffness leads to a drag knee-point occurring at a lower pressure and increased friction pad stiffness moves the drag knee-point to a higher pressure, see Figure 4.3. Inner and outer pad drag torque values are referenced in Table 4.1.

BRAKE PRESSURE (bar)	BASELINE MODEL (Drag Torque-Nm)		INCREASED FRICTION PAD STIFFNESS (Drag Torque-Nm)		DECREASED FRICTION PAD STIFFNESS (Drag Torque-Nm)	
	Inner pad	Outer pad	Inner pad	Outer pad	Inner pad	Outer pad
2	0	0	0	0	0	0
4	0	0	0	0	0	0.120
6	0	0.339	0	0.212	0	0.799
8	0	0.877	0	0.601	0	1.715
10	0	1.554	0	1.137	0	1.925
15	0	1.924	0	1.919	0	1.926
20	0	1.922	0	1.925	0	1.925
30	0	1.927	0	1.929	0	1.924
40	0	1.929	0	1.932	0	1.925
50	0	1.930	0	1.936	0	1.924
60	0	1.931	0	1.940	0	1.923
70	0	1.932	0	1.943	0	1.922
80	0	1.935	0	1.946	0	1.924
90	0	1.941	0	1.946	0	2.019
100	0	1.942	0	1.951	0	2.451
120	0.177	2.124	0	1.955	Convergence Issue	Convergence Issue
140	Convergence Issue	Convergence Issue	0.292	2.259	Convergence Issue	Convergence Issue

Table 4.2: Brake drag torque for modified friction pad stiffness compared to base line model

4.2.3 Effect of omega spring stiffness

From Figure 4.4 it is noted that both curves have a similar trend line as in previous simulations. However a closer look, reveals that the initial drag torque peak caused by the new friction pad lining at 0 - 15 bar has been drastically reduced from 1.8Nm to 0.7Nm at lower pressure. As shown in the Table 4.3 drag torque until 120 bar is recorded and convergence issue is observed at 140 bar of pressure.

Qualitative analysis on parametric study simulations shows that modified caliper housing and friction pad stiffness give better longitudinal flexibility. Increasing the stiffness on both components made the drag knee-point occur at higher brake pressures. This leads to a decrease in brake drag torque. Lastly, decreased omega spring stiffness provides less pretension forces on neighbouring components which reduces brake drag torque.

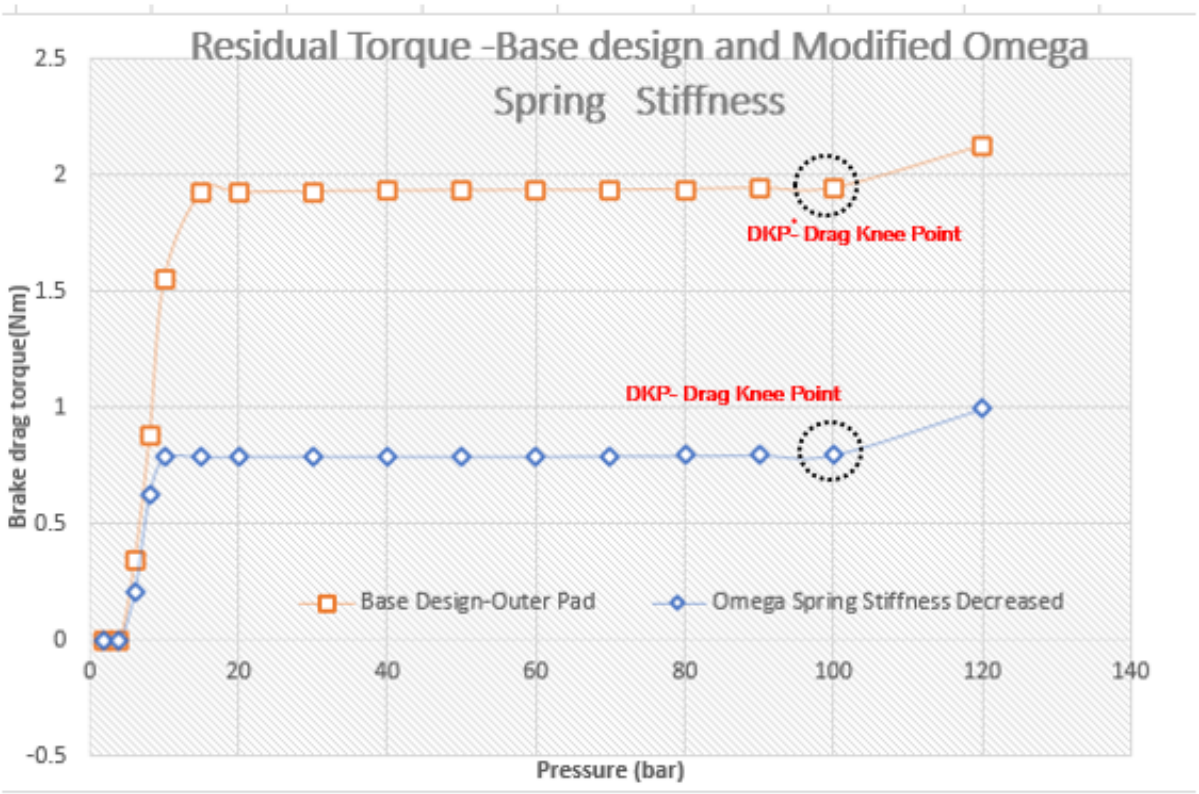

Figure 4.4: Simulation results for modified omega spring stiffness compared to base line model

BRAKE PRESSURE (bar)	BASELINE MODEL (Drag Torque-Nm)		DECREASED OMEGA SPRING STIFFNESS (Drag Torque-Nm)	
	Inner pad	Outer pad	Inner pad	Outer pad
2	0	0	0	0
4	0	0	0	0.202
6	0	0.339	0	0.204
8	0	0.877	0	0.624
10	0	1.554	0	0.784
15	0	1.924	0	0.787
20	0	1.922	0	0.790
30	0	1.927	0	0.790
40	0	1.929	0	0.790
50	0	1.930	0	0.791
60	0	1.931	0	0.790
70	0	1.932	0	0.792
80	0	1.935	0	0.793
90	0	1.941	0	0.795
100	0	1.942	0	0.797
120	0.177	2.124	0.183	0.997
140	Convergence Issue	Convergence Issue	Convergence Issue	Convergence Issue

Table 4.3: Brake drag torque for decreased omega spring stiffness compared to base line model

5

Conclusion and Future Work

5.1 Conclusion

The FEM validation tool, i.e., Abaqus enabled modelling of the complex non-conservative forces. Further, it helped in adapting the specifications of a generic friction brake assembly. This proved to be useful in calculating the drag torque. This complete modelling and simulation setup was used to achieve the quantification of residual torque. Further, it aided in determining the critical factors that influence the brake drag torque.

In this work, Marlow's hyperelastic material model was used to model realistic behaviour of rubber and it improves the accuracy of the simulated drag torque. Preliminary simulations were carried out for a baseline friction brake assembly which was used to draw qualitative conclusions regarding associated components. There were limitations in loading the assembly with higher level of pressure due to static instabilities caused by unconstrained rigid body modes. Belief in the model was fortified by observing the generic behaviour of the brake. This behaviour was compared with existing research data by plotting graphs of drag torque at respective brake pressures. This accuracy of quantifying the drag torque laid path to the parametric study of the influencing factors.

The caliper housing stiffness and the friction pad stiffness were considered to be major parameters influencing when comparing to the baseline model. However, this was already highlighted in several research papers found in the literature survey. A very interesting observation made during the baseline study was the unexpected impact of the omega spring's deflection behaviour. Hence, this was incorporated in the parametric study by playing with the values of the stiffness of this component. This proved to be useful as the brake drag torque was reduced by almost 50% in low pressure range. Though drag torque was reduced, the trend was in-line with the observations made when only caliper housing stiffness and friction pad stiffness were varied, i.e., drag knee-points were advanced or delayed. This also concluded that the influence of retraction of the seal was independent of the stiffness i.e., the knee-point occurred in all simulations. It was also observed that the inner pad drag torque follows the same trend as the outer pad drag torque.

The virtual environment model that was developed in this thesis will help in modelling and simulating multiple design prototypes in a shorter time-frame. This will

lead to reduced development time without compromising on accuracy and efficiency and also achieve drag torque reduction and optimal brake performance.

5.2 Future scope

A reliable finite element model of a friction brake assembly was achieved in this thesis work. It was developed to correlate to real time physical testing. The robustness, or rather the stability, of the model needs improvement at higher brake pressures by having a more accurate hyperelastic material model and less static instabilities. A parametric study of some further influencing factors needs to be carried out. A higher degree of accuracy in simulation results can be approached by analysing different friction brake assembly designs. For a better assessment the parametric study of factors influencing drag torque should also include aspects as squeal noise, durability and efficiency of braking.

Bibliography

[1] Backstrom, A., "Brake Drag Fundamentals," SAE Technical Paper 2011-01-2377, 2011.

[2] Reich, A., Sarda, A., and Semsch, M., "Drag Torque in Disk Brakes: Significance, Measurement and Challenges," SAE Int. J. Commer. Veh. 8(2):276-282, 2015.

[3] Anwana, O., Cai, H., and Chang, H., "Analysis of Brake Caliper Seal-Groove Design," SAE Technical Paper 2002-01-0927, 2002.

[4] Day, A., Ho, H., Hussain, K., and Johnstone, A., "Brake System Simulation to Predict Brake Pedal Feel in a Passenger Car," SAE Technical Paper 2009-01-3043, 2009.

[5] Cai, H. and Anwana, O., "Seal/Groove Performance Analysis Models," SAE Technical Paper 2002-01-2588, 2002.

[6] Antanaitis, D., "Vehicle Integration Factors Affecting Brake Caliper Drag," SAE Int. J. Passeng. Cars - Mech. Syst. 5(4):1244-1258, 2012.

[7] Brake Caliper Piston Seals (Visited on 18/3/2022)

[8] Reich, A., Sarda, A., and Semsch, M., "Drag Torque in Disk Brakes: Significance, Measurement and Challenges," SAE Int. J. Commer. Veh. 8(2):2015, doi:10.4271/2015-01-2670.

[9] FEA, Structural integrity, Mechanical Eng Basic Theory, etc (Visited on 9/2/2022).

[10] Massachusetts Institute of Technology. “Contact formulations in Abaqus/Standard.” (2017)

[11] abaqus-advanced-contact (visited on 15/03/2022)

[12] Massachusetts Institute of Technology. “Contact constraint enforcement methods in Abaqus/Standard.” (2017) (visited on 27/03/2022)

[13] Massachusetts Institute of Technology. “ Contact pressure definition” (2017) (visited on 30/03/2022)

[14] Massachusetts Institute of Technology. “Contact pressure-overclosure relationships” (2017) (visited on 30/03/2022)

[15] Massachusetts Institute of Technology. “ Defining hyperelastic behavior using test data” (2017) (visited on 30/03/2022)

[16] Hyperelastic material models in Abaqus (visited on 30/03/2022)

DEPARTMENT OF MECHANICS AND MARITIME SCIENCES
CHALMERS UNIVERSITY OF TECHNOLOGY
Gothenburg, Sweden
www.chalmers.se

CHALMERS
UNIVERSITY OF TECHNOLOGY